Parameterization of PBL processes in an Atmospheric General Circulation Model: Description and Preliminary Assessment

Celal S. Konor*, Gabriel Cazes Boezio†, Carlos R. Mechoso[‡] and Akio Arakawa[‡]

* *Department of Atmospheric Science, Colorado State University*

† *IMFIA, Universidad de la República, Uruguay*

[‡] *Department of Atmospheric and Oceanic Sciences, University of California Los Angeles*

September 2008

Corresponding author address:
Dr. Celal S. Konor
Department of Atmospheric Science
Colorado State University
Fort Collins, Colorado, 80523-1371
Email: csk@atmos.colostate.edu

ABSTRACT

This paper presents the basic features of a newly developed planetary boundary layer (PBL) parameterization, and the performance assessment of a version of the UCLA Atmospheric General Circulation Model (AGCM) to which the parameterization is incorporated. The UCLA AGCM traditionally uses a framework in which a sigma-type vertical coordinate for the PBL shares a coordinate surface with the free atmosphere at the PBL top. This framework facilitates an explicit representation of processes concentrated near the PBL top, which is crucially important especially for predicting PBL clouds. In the new framework, multiple layers are introduced between the PBL top and Earth's surface, allowing for predictions of the vertical profiles of potential temperature, total water mixing ratio and horizontal winds within the PBL. The vertically integrated "bulk" turbulent kinetic energy (TKE) is also predicted for the PBL. The PBL-top mass entrainment is determined through an equation including the effects of TKE and the radiative and evaporative cooling processes concentrated near the PBL top. The surface fluxes are determined from an aerodynamic formula in which the velocity scale depends both on the square root of TKE and the grid-scale PBL velocity at the lowermost model layer. The turbulent fluxes within the PBL are determined through an approach that includes the effects of both large convective and small diffusive eddies.

AGCM simulations with the new formulation of PBL are analyzed with a focus on the seasonal and diurnal variations. The simulated seasonal cycle of stratocumulus over the eastern oceans is realistic, so are the diurnal cycles of the PBL depth and precipitation over land. The simulated fluxes of latent heat, momentum and short wave radiation at the ocean surface and

baroclinic activity in the middle latitudes show significant improvements over the previous versions of the AGCM based on the single-layer PBL.

1. Introduction

Planetary boundary layer (PBL) processes play an important role in general circulation of the atmosphere by controlling the transfer of momentum, heat and water vapor from the underlying Earth's surface. These transfer processes can generally be characterized as complex physical and dynamical interactions dominated by turbulent transport and mixing. Atmospheric general circulation models (AGCMs) used for climate studies must correctly represent such complex interactions. The vertical resolution of AGCMs, however, generally does not suffice to explicitly resolve the vertical structure of PBL processes. A parametric representation of those processes, therefore, is needed for practically all AGCMs. The main objectives of a PBL parameterization are 1) estimation of the surface fluxes of prognostic variables, 2) determination of whether or not the PBL has clouds and formulation of processes associated with clouds, and 3) formulation of the interactions between PBL and the free atmosphere. A realistic simulation of the cloud-topped PBL processes is particularly important in the case of atmosphere-ocean coupled simulations because the deficiencies in simulating cloud-radiation/turbulence/thermodynamics interactions can easily lead to spurious feedbacks through errors in predicted sea surface temperature (SST). Ma et al. (1996) demonstrates the importance of these interactions over the eastern tropical Pacific.

Commonly used PBL schemes usually specify the vertical profile of turbulent diffusivity. Most of the earlier schemes are "local" in the sense that the eddy diffusivity depends on the local vertical shear and static stability (e. g., Louis 1979; Louis *et al*. 1982). Many of the more recent schemes are "non-local" in the sense that eddy diffusivity is controlled by the surface heat flux with a prescribed vertical profile (e.g., Troen and Mahrt 1986; Holtslag *et al*. 1990; Holtslag and Boville, 1993). In these schemes, the height of the PBL top is

diagnostically determined without explicitly considering the mass entrainment through the PBL top. Holtslag and Boville (1993) compared the results obtained by the NCAR Community Climate Model using local and non-local schemes. They concluded that the non-local schemes represent the dry PBL processes better than the local schemes.

In the PBL parameterizations mentioned above, PBL clouds are usually determined by an empirical diagnosis based on relative humidity (Sundqvist 1978; Slingo *et al.* 1982; Smith 1990) or prediction of cloud liquid water (LeTreut and Li 1991; Del Genio *et al*. 1996). None of these diagnostics considers the interactions between cloud radiation and turbulence although these processes play a crucial role in generation and maintenance of the extensive cloud decks over cold oceans. The scheme by Lock *et al.* (2000) uses different diffusivity profiles depending on cloud regimes so that interactions between cloud radiation and turbulence can be included if a sufficiently high vertical resolution is employed. Martin *et al.* (2000) demonstrates the effectiveness of this scheme in simulating cloud amounts and PBL structures.

An alternative approach is based on the mixed-layer formulation (Lilly 1968). In this approach, the PBL depth is explicitly predicted using the layer's mass budget (e.g., Randall 1976; Suarez *et al*. 1983; Randall et al. 1989; Tokioka *et al*. 1984; see also Arakawa 2004). This prediction requires estimation of the mass entrainment through PBL top. For a cloud-free PBL, such entrainment formulation is well established (e.g., Deardorff 1972). For a cloud-topped PBL several formulations have been proposed (e.g., Lock 1998, Turton and Nicholls 1987, Moeng 2000, Lilly 2002; and Randall and Schubert 2004). Most of these formulations consider the fraction of the buoyancy flux needed to overcome the effect of stratification at cloud top on the entrainment rate (see Stevens 2002).

A very attractive aspect of PBL schemes based on the mixed-layer approach is that interactions with the free atmosphere and processes associated with the PBL-top clouds can be

explicitly formulated. The PBL-top clouds form above the lifting condensation level within the PBL and they are assumed to individually or together represent stratocumulus, stratus and fog (if the cloud bottom extends to the ground) as observed in Nature. We will refer those three types of clouds simply as "stratocumulus" clouds in the rest of this paper. The radiative cooling at the top of stratocumulus clouds contributes to the generation of turbulence and the mass entrainment from the free atmosphere. These interactions are crucial for the maintenance of stratocumulus decks in the areas under large-scale subsidence and/or over cold SST.

In the framework traditionally used in the UCLA AGCM, the lowest model layer is assigned to the PBL (Suarez *et al*. 1983). The depth of this layer is predicted through the mass budget equation including the PBL-top entrainment, cumulus mass flux and horizontal mass convergence within the PBL. When the entrainment and cumulus mass flux become zero, the PBL-top becomes a material surface, keeping the PBL air separated from the free atmosphere air. The UCLA AGCM using this framework has been applied to many climate studies, particularly in research on air-sea interactions for which the AGCM was successfully coupled to ocean GCMs (Mechoso *et al*. 2000). Motivated by this success, Konor and Arakawa (2005) introduced a new framework, which maintains the advantages of the mixed-layer formulation while relaxing the mixed-layer constraint by introducing several layers within the PBL. Figure 1 is a schematic depiction of this framework. Explicit prediction of vertical shear within the PBL is expected to have a major impact on the evolution of extratropical baroclinic disturbances. It also has a potential for capturing the rich variety of cloud types in the tropics, such as those described by TRMM data and the data gathered during an EPIC 2001 cruise (Bretherton et al. 2004).

The PBL scheme of Konor and Arakawa (2005 and 2008) has aspects in common with the one proposed by Grenier and Bretherton (2001). The latter scheme also predicts the height of

the inversion layer that caps a convective PBL using the mass budget equation, as in the mixed-layer formulation. The internal vertical structure of the PBL is then obtained by using turbulent fluxes computed with a 1.5-order closure based on Mellor and Yamada (1982). Tests of the scheme using a single column model with both coarse and fine vertical resolutions showed that it could successfully simulate the dry-convective PBL with both resolutions. However, simulation of the cloud-topped PBL was found satisfactory only for resolutions of 15 hPa or less. A major difference between Konor-Arakawa and Grenier-Bretherton schemes is that the PBL top in the former shares a coordinate surface with the free atmosphere, while in the latter the PBL top floats between model's coordinate surfaces.

In the new framework being presented here, PBL processes are parameterized following a new approach. The effects of large convective eddies are represented by a bulk formulation, which includes prediction of TKE, and the effects of small eddies that are mostly diffusive are represented by a K-closure formulation that uses a diffusivity coefficient profile based on Holtslag and Boville (1993). The PBL-top mass entrainment is explicitly computed with a formulation proposed by Randall and Schubert (2004). The surface fluxes of momentum, heat and water vapor are determined by an aerodynamic formula, in which both the square root of TKE and the mean large-scale PBL velocity are used to determine the velocity scale. With this formulation, the surface fluxes estimates are expected to be better than the traditional methods because the grid-scale wind can be weak while the convective mixing is strong.

The new PBL parameterization scheme is tested with the uncoupled and coupled climate simulations. The present paper illustrates the behavior of the PBL in an actual climate simulation with the uncoupled UCLA AGCM. While the comparison between simulation and observation can tell us a great deal about the overall quality of the PBL parameterization scheme, it alone cannot confirm the impact of individual processes or interactions. We

therefore show results from two additional experiments. In the first experiment, the effects of radiative cooling at the PBL top (in the presence of PBL clouds) on TKE generation and entrainment rate are turned off. This experiment is extended by additionally eliminating the effect of radiative cooling on the potential temperature of the uppermost PBL layer. In the second experiment, the model's vertical structure is changed to the conventional sigma coordinate, i.e. the definition of sigma levels are independent of the PBL top. In this case, the PBL depth and turbulent fluxes are determined through the diagnostic equation given by Troen and Mahrt (1986) and the non-local flux formulation proposed by Holtslag and Boville (1993), respectively.

The PBL parameterization we are presenting in this paper does not fully benefit from the potential of the multi-layer framework. We believe that the benefit of the multi-layer framework is not fully realized before we predict TKE for each layer and incorporate a scheme to represent cumulus roots. At this stage, what we can realistically expect from the multi-layer framework is an improvement in the simulated vertical wind shear within the PBL and, as a consequence, the effect of low-level baroclinicity.

The text of the paper is organized as follows. Section 2 briefly describes the AGCM and presents a description of the new PBL parameterization. Section 3 shows the results of a multi-year simulation with the model. Section 4 presents the cloud-radiation/turbulence/thermodynamics interactions with the new PBL parameterization, and discusses the results of experiments that demonstrate the importance of those interactions. Comparisons of the results obtained using new and previous parameterizations are also presented in section 4. Section 5 compares the results obtained by a first-order turbulence closure scheme with diagnostic determination of clouds and our new PBL parameterization

scheme. Section 6 gives a summary and discussion of the results, and a preview of developments.

2. Brief Description of the AGCM and the PBL parameterization

a. Outline of the UCLA AGCM

The UCLA AGCM is a global model that integrates the primitive equations for the atmosphere. The model's horizontal and vertical discretizations are based on the Arakawa C grid and the Lorenz grid, respectively (Arakawa and Lamb 1977; Arakawa and Suarez 1983). Parameterization of physical processes other than those of the PBL include solar and terrestrial radiation following Harshvardhan *et al*. (1987 and 1989, respectively) and a prognostic version of the Arakawa and Schubert (1974) cumulus convection scheme presented by Pan and Randall (1998). In this scheme, the original assumption of quasi-equilibrium for the cloud work function is relaxed by predicting the cloud-scale kinetic energy.

The vertical coordinate system used in the model is presented in Suarez *et al*. (1983). The vertical domain is divided into three regions (Fig. 2), the boundaries of which are coordinate surfaces. The highest region extends from the model's top ($p_T = 1\text{hPa}$) to the mean tropopause level ($p_I = 100\ \text{hPa}$). The middle region extends from the mean tropopause level down to the PBL top (p_B), which varies in space and time. The lowest region represents the PBL. Within these regions, the definition of vertical sigma coordinate is given by,

$$\sigma_{stra} \equiv (p - p_I)/(p_I - p_T) \quad \text{for } p_T \le p \le p_I, \tag{1a}$$

$$\sigma_{trop} \equiv (p - p_I)/(p_B - p_I) \quad \text{for } p_I \le p \le p_B \tag{1b}$$

and

$$\sigma_{pbl} \equiv 1 + (p - p_B)/(p_S - p_B) \text{ for } p_B \le p \le p_S, \quad (1c)$$

where p_S is the surface pressure. Accordingly, $\sigma = 2$ at the Earth's surface, $\sigma = 1$ at the PBL top, $\sigma = 0$ at the mean tropopause level, and $\sigma = -1$ at the model's top.

The coordinate surface at the PBL top ($\sigma = 1$) represents an infinitesimally thin transition layer that separates the PBL air below from the free atmosphere air above. The quantities on the upper and lower boundaries of this layer are determined by extrapolations from the inner part of the corresponding regions. The PBL depth $(\delta p)_{PBL} \equiv p_S - p_B$ is predicted through the mass budget equation by taking into account the entrainment and cumulus mass flux at the PBL-top, and the vertically integrated horizontal mass convergence within the PBL. The vertical mass flux through coordinate surfaces within the PBL is obtained by a diagnostic equation consistent with the definition of sigma given by (1c). Then, the potential temperature (θ) and total water-mixing ratio ($r \equiv q + \ell$, where q and ℓ are water vapor and liquid water mixing ratios, respectively) are predicted for all PBL layers. A detailed description of the discretization of these prognostic equations with the sigma coordinate is given in Konor *et al*. (2004).

b. Parameterization of PBL processes

Konor *et al*. (2004) and Konor and Arakawa (2008) describe in detail the PBL parameterization scheme for the coordinate system described by (1a) to (1c) and a generalized vertical coordinate. In this subsection we outline the main aspects of the parameterization in reference to that used in previous versions of the UCLA AGCM.

i) Prediction of vertically averaged TKE

The vertically averaged turbulence kinetic energy in the PBL (e_{PBL}, TKE) is explicitly predicted through

$$\frac{\partial e_{PBL}}{\partial t} = -\frac{e_{PBL}}{(\delta p)_{PBL}} gE + \frac{g}{(\delta p)_{PBL}}(\mathcal{B} + S - \mathcal{D}) + \frac{e_{PBL}}{(\delta p)_{PBL}} \nabla \cdot \left[(\delta p)\mathbf{v}\right]_{PBL}, \qquad (2)$$

where E is the PBL-top entrainment, which will be discussed later, g is gravitational acceleration; $\mathcal{B}$, S and $\mathcal{D}$ represent buoyancy generation, shear generation, and dissipation, respectively. We follow Krasner (1993) for derivation, Randall *et al.* (1992) for usage, and Moeng and Sullivan (1994) for dissipation. The buoyancy generation is determined from $\mathcal{B} \equiv \int_{p_B}^{p_S} \kappa F_{sv} d\ell np$, where p is the pressure; S and B denote surface and PBL top, respectively; $\kappa = R/c_p$, R is the gas constant, c_p is the specific heat of dry air under constant pressure; F_{sv} is the turbulent flux of the dry virtual static energy $s_v \equiv c_p T_v + gz$, where $T_v \equiv T(1 + 0.608q - \ell)$ is the virtual temperature, where T is the temperature. At the surface and PBL top, F_{sv} is defined by $(F_{sv})_S \equiv (F_h)_S + (0.608\Pi_S \theta_{PBL} - L)(F_q)_S$ and $(F_{sv})_{B^-} \equiv -E\left[(\Delta h)_B + (\Delta R)_B + (0.608\Pi_B \theta_{PBL} - L)(\Delta r)_B\right]$, where B^- denotes the lower boundary of the transition layer at the top of PBL. In these equations, F_h is the turbulent flux of moist static energy $h \equiv c_p T + gz + Lq$; F_q is the turbulent flux of water vapor; $\Pi \equiv c_p (p/p_0)^{R/c_p}$ is the Exner function; θ_{PBL} is mean potential temperature within the subcloud layer of the PBL; and L is the latent heat of evaporation; $(F_h)_S$ and $(F_q)_S$ are the surface fluxes of h and q respectively, determination of which discussed in subsection (iv); E is the

entrainment rate discussed in the next subsection; $(\Delta\psi)_B \equiv \psi_{B^+} - \psi_{B^-}$ is commonly called the jump of ψ at the PBL-top, where the subscript B^+ upper boundary of the transition layer at the top of PBL; $(\Delta R)_B$ is the radiation jump at the PBL top for a cloud-topped PBL. (Positive values of the radiation jump correspond to radiative cooling.) The reader is referred to Konor and Arakawa (2008), Suarez *et al*. (1983) and Randall (1976 and 1980b) for more details. To summarize, the buoyancy generation includes the effects associated with the upward buoyancy flux from the earth's surface through positive values of $(F_{sv})_S$ and, in the case of a cloud-topped PBL, the net long wave radiative cooling at the PBL top through positive values of $(\Delta R)_B$; the buoyancy destruction includes the effects of entrainment of warmer and drier air from the free atmosphere through positive values of $E(\Delta h)_B$ and the downward buoyancy flux from the earth's surface through negative values of $(F_{sv})_S$. In our application of the TKE prediction equation, we add the last term in (2) to represent a dilution (concentration) effect when PBL deepens (shallows) due to horizontal mass convergence (divergence). It is assumed that the predicted PBL TKE and depth cannot be lower than prescribed values [$(e_{PBL})_{min} = 10^{-3}\,\mathrm{m^2 sec^{-2}}$ and $(\delta p_{PBL})_{min} = 10\,\mathrm{mb}$, respectively].

ii) Turbulent fluxes within the PBL

The turbulent fluxes are determined following a hybrid approach. For conserved quantities, such as those of moist static energy *h* and total water mixing ratio *r*, turbulent fluxes due to large eddies (with a length-scale of the order of PBL height) are determined from

$$F_\psi \equiv \frac{\sigma - \sigma_B}{\sigma_S - \sigma_B}\left(F_\psi\right)_S + \frac{\sigma_S - \sigma}{\sigma_S - \sigma_B}\left(F_\psi\right)_{B^-}, \tag{3}$$

where ψ is *h* or *r*, and *S* and B^- denote the surface and upper boundary of PBL, respectively. The formulations of turbulent fluxes at the surface in (3) are discussed later in this text. Fluxes at the PBL top are obtained from definitions given in previous paragraph.

The turbulent fluxes of conserved quantities due to small eddies are determined by a K-closure given by

$$\tilde{F}_\psi \equiv -\rho K_\psi \left(\frac{\partial \psi}{\partial z} - \gamma_\psi \right), \tag{4}$$

where ρ is density, *z* is height, K_ψ is diffusion coefficient, and γ_ψ is transport. For the latter two, we use a scheme based in Troen and Mahrt (1986) and Holtslag and Boville (1993) with a modified turbulent velocity scale that depends on predicted TKE. This modification is done because, within a convective mixed layer, small eddies are generated primarily through the energy cascade from larger eddies and, therefore, their properties should depend on the bulk parameters such as TKE and the PBL height. Since (4) is applied to small eddies only that are assumed to be mostly diffusive in our parameterization, we use a fraction of γ_ψ suggested by the formulation of Troen and Mahrt (1986). For saturated layers, we used a large constant value for the diffusion coefficient in order to represent the strong mixing within clouds. The potential temperature fluxes due to large and small eddies are calculated from the fluxes of *h* and *r*, through

$$\left.\begin{aligned} F_\theta &\equiv \frac{1}{\Pi}\left(F_h - LF_r\right) \ \textit{for an unsaturated layer} \\ F_\theta &\equiv \frac{1}{\Pi\left(1+\gamma^*\right)}F_h \ \textit{for a saturated layer} \end{aligned}\right\}, \tag{5}$$

where p_0 is a standard pressure; and $\gamma^* \equiv \frac{L}{c_p}\left(\partial q^* / \partial T\right)_p$. Within a saturated layer subject to turbulent mixing, the potential temperature increases roughly linearly with height due to the heat released by the condensation process. Through the term with γ^* in (5), the effect of condensation heating on the potential temperature profile is automatically included.

The effects of sub-grid scale orography on the breaking of stratocumulus clouds are parameterized according to Terra (2004). At this point, we are not including a separate parameterization scheme for shallow cumulus clouds. Transition to the shallow cumulus regime from unbroken stratocumulus deck is parameterized through the cloud-top entrainment instability (CTEI) process (Randall 1976; 1980a,b; Deardorff 1980). Inclusion of a shallow-cumulus parameterization scheme is among our future plans.

iii) Entrainment rate at the PBL top

The entrainment rate through the PBL top is computed from the formulation based on the work by David Randall *et al*. in 1990s (Randall and Schubert 2004) inspired by the ideas of Breidenthal and Baker (1985), Siems *et al*. (1990) and Breidenthal (1992). A review of entrainment formulations, including the one we discuss here, can be found in Stevens (2002). Our version has minor modifications from the original one in order to improve consistency with the predicted TKE:

$$E = \frac{b_1 \rho_{PBL} \sqrt{\tilde{e}_{PBL}} + \tilde{b}_2 \beta_B g \left[\frac{(\delta z)_{PBL}}{e_{PBL}}\right] \frac{(\Delta R)_B}{\Pi_B \theta_{PBL}}}{1 + b_2 g \left[\frac{(\delta z)_{PBL}}{e_{PBL}}\right] \frac{(\Delta s_v)_B - \Delta s_{v_{crit}}}{\Pi_B \theta_{PBL}}}, \qquad (6)$$

where ρ_{PBL} is the mean density within the PBL, the subscript *B* denotes the PBL-top, $\beta \equiv \frac{1}{1+\gamma^*}\left(1+1.608\gamma^* c_p T/L\right)$, $(\delta z)_{PBL}$ is height of PBL top form the surface, $\left(\Delta s_v\right)_B$ is PBL-top jump of the virtual dry static energy and $\Delta s_{v_{crit}}$ is the critical virtual dry static energy jump originally defined by Randall (1980a). Our use of $\tilde{e}_{PBL} \equiv e_{PBL} - \left(e_{PBL}\right)_{min}$ and $\tilde{b}_2 \equiv b_2\left\{1 - exp\left[-0.1\tilde{e}_{PBL}/\left(e_{PBL}\right)_{min}\right]\right\}$ instead of e_{PBL} and b_2, respectively, guarantees that $E \to 0$ as $e_{PBL} \to \left(e_{PBL}\right)_{min}$. In these equations, b_1 and b_2 are 0.4 and 0.8, respectively.

In summary, the entrainment rate is computed as a function of TKE and a bulk Richardson number defined in terms of TKE and the inversion strength represented by $\left(\Delta s_v\right)_B$. In the case of a cloud-topped PBL, the calculation uses an "effective Richardson number" based on an "effective" inversion strength, which takes into account the effects of radiative and evaporative cooling at cloud top represented by $\left(\Delta R\right)_B$ and $\left(\Delta s_v\right)_B - \Delta s_{v_{crit}}$, respectively, on the turbulent flux of buoyancy. During collapse, entrainment is replaced by a rapid detrainment to simulate the disappearance of a well-defined PBL top after sunset over land.

iv) Turbulent fluxes of momentum, sensible and latent heat at Earth's surface

The turbulent surface fluxes of momentum, temperature and water vapor at Earth's surface are determined from an aerodynamic formula. This is a modification of the one proposed by Deardorff (1972), in which the surface flux of a variable depends upon the deficit of its mean PBL value in reference to the Earth's surface.

In our formulation, the velocity scale is taken as the maximum between the square root of TKE and the modulus of the large-scale PBL velocity at the lowermost layer, both weighted by empirical coefficients. The reader is referred to Zhang *et al.* (1996) for the use of the square

root of TKE as the velocity scale in the surface flux formulation. The surface fluxes obtained in this way are expected to be better than those obtained with more traditional methods in regions where the mean wind can be weak while convective mixing is strong. The fluxes of momentum, temperature and water vapor are given by the following relationships:

$$\left.\begin{aligned} \left(\mathbf{F}_{\mathbf{v}}\right)_S &\equiv -\rho_S C_U C_U \,\mathrm{Max}\left\{\alpha_1 |\mathbf{v}_L|,\, \beta_1 e_{PBL}^{1/2}\right\}\mathbf{v}_L \\ \left(F_\theta\right)_S &\equiv \rho_S C_U C_T \,\mathrm{Max}\left\{\alpha_2 |\mathbf{v}_L|,\, \beta_2 e_{PBL}^{1/2}\right\}\left(\theta_S - \theta_L\right) \\ \left(F_q\right)_S &\equiv \rho_S C_U C_T \,\mathrm{Max}\left\{\alpha_2 |\mathbf{v}_L|,\, \beta_2 e_{PBL}^{1/2}\right\}\left[q^*\left(T_S, p_S\right) - q_L\right] k \end{aligned}\right\}, \qquad (7)$$

where ρ_S is the density at the lowest PBL layer, C_U and C_T are surface exchange coefficients computed following Deardorff (1972), $\mathbf{v}$ is vector wind velocity, the subscript L denotes the lowermost PBL layer, θ_S , T_S and p_S are potential temperature, surface temperature, and pressure at the Earth's surface, respectively, and k is a coefficient that represents ground wetness. The coefficient k is set one for water surfaces, and to a value close to zero for arid lands. The parameters α_1, β_1 , α_2 and β_2 are scale coefficients empirically determined to obtain realistic simulated fluxes. We are currently using $\alpha_1 = 1.0$, $\beta_1 = 5.5$, $\alpha_2 = 0.7$, $\beta_2 = 4.0$.

3. Selected results of the AGCM with the new PBL parameterization

The PBL parameterization described in Section 2 was incorporated into the UCLA AGCM. To illustrate the performance of the revised model, we carried out simulations in an uncoupled mode with prescribed sea surface temperatures (SST). These simulations are 5-year long and use the low-resolution version of the AGCM with the 5^o long. by 4^o lat. horizontal

resolution with 18 layers (4 in the PBL). The initial condition corresponds to November 30 in a long-term run of a previous model version with the same resolution, but using a single-layer PBL. The SST, sea-ice, Earth's surface albedo and roughness, and ground wetness distributions are obtained daily by linear interpolation from the twelve monthly means of observed climatologies taken from the Global Sea-Ice and SST Data Set (Rayner *et al*. 1995) for sea-ice and SST, and Dorman and Sellers (1989) for surface albedo and roughness. We show the averages of monthly means over a 5-year period. Our emphasis in this section is on those fields that are directly influenced by the PBL scheme.

a. Global surface fields

We start by inspecting the simulated monthly-mean sea level pressure. Figure 3 shows the distributions for January and July (left and right columns, respectively) from the NCEP reanalysis (Kalnay *et al*. 1996) and the simulation (upper and lower rows, respectively). The simulation clearly reproduces the main features of the observed climatology, such as the subtropical highs in the Northern Hemisphere during summer, the Aleutian low during winter, and the subtropical highs in the Southern Hemisphere both in winter and summer. In January, the simulated sea level pressure over the continents in the Northern Hemisphere tends to be lower than in the NCEP reanalysis. Note that the differences between the observation and simulation over Tibetan plateau are influenced by the method used to obtain sea level values in regions of high terrain. The simulated low-pressure belt around Antarctica is too weak in both January and July, which is a feature fairly common to AGCMs with low horizontal resolution (Boville 1991).

Figure 4 shows the simulated monthly-mean PBL depth, TKE, and stratocumulus clouds incidence (as the percentage of time of occurrence) for January, April, July and October. The

PBL depth (left column in Fig. 4) is generally lower over the continents than over the oceans. This is due to the strong diurnal cycle of PBL over land, with very shallow PBLs during nighttime over cold ground, although PBLs can be very deep during daytime as solar radiation warms the surface. Over the oceans, there are local maxima along the major storm tracks, particularly during winter. The PBL tends to be deep in the subtropical and tropical regions with high incidence of marine stratocumulus clouds. In the western tropical oceans, cumulus activity prevents PBL from becoming too deep. TKE (central column) over the oceans has local maxima at locations that approximately coincide with those of larger PBL depth and stratocumulus incidence (right column). Over the continents, the local maxima of TKE tend to be in the regions with either convectively unstable PBL during daytime or with high low-level winds over rough surface (not shown). The geographic distribution and seasonal cycle of simulated stratocumulus clouds are consistent with the observation (e.g., Klein and Hartmann 1993). The eastern parts of the subtropical oceans show high stratocumulus incidence that characterizes the climate of those regions. In the northeastern Pacific, stratocumulus incidence is maximum in July and minimum in January (Figs. 4*i* and 4*k*). In the southeastern Pacific and Atlantic, the maximum is in October and the minimum in April (Figs. 4*j* and 4*l*). The simulation also shows high stratocumulus incidence along the major storm tracks; this feature is consistent with the climatology of Klein and Hartmann (1993).

The approximate collocation of larger values in PBL depth, TKE, and stratocumulus incidence over oceans suggests the interdependence between these variables. The results obtained fit the following scenario. Higher values of TKE tend to produce deeper PBLs, which favor higher stratocumulus incidence. In turn, higher radiative cooling associated with stratocumulus tends to increase TKE, which sets up a positive feedback. These aspects are further discussed in section 4.

We next concentrate on the surface fluxes of heat and water vapor. Latent heat flux provides one of the largest contributions to the net heat flux over the tropical and subtropical oceans. Figure 5 shows the observed upward latent heat flux from the COADS analysis (Da Silva *et al*. 1994) averaged from 1979 to 1993 for January (a), July (c), and the corresponding simulated fields ((b) and (d), respectively). In general, the simulation reproduces the observed patterns reasonably well. For example, the relatively large values tend to occur over the subtropical oceans of the winter hemisphere. In January, the strong fluxes from the warm waters of the Kuroshio Current and Gulf Stream are well captured. The simulated values are too strong at spots in the Bay of Bengal and off the Pacific coast of Central America, and in the central part of the subtropical North Atlantic. Otherwise, differences (not shown) between simulation and analysis are generally one order of magnitude smaller than the actual fields. In July, the simulated latent heat flux distribution compares reasonably well to the observed one.

The net solar radiation flux is the most important contribution to the heat flux into the ocean, and the PBL clouds directly affect its values. Figure 6 shows the monthly-mean fields for January and July from the NASA SRB Analysis (http://srb-swlw.larc.nasa.gov/ GEWEX_SRB_ homepage.html) averaged from 1983 to 1991 (left column, lower and upper panels, respectively) and from the simulation (right column, upper and lower panels, respectively). A comparison of Fig. 6a to b shows that the simulation reproduces the observed patterns reasonably well for January except that the amplitude of simulated values tends to be too large over the Indian Ocean. For July, the simulations (Fig. 6d) tend to yield larger values than observation (Fig. 6c) off the coasts of California and Peru where the simulated stratocumulus incident is high (see Fig. 4*i*). This may indicate that the stratocumulus clouds appear more transparent than they should be to the radiation parameterization in the model. This is one of the issues that we will address in our future revisions.

b. Vertical Profiles of Thermodynamic Variables over Ocean

Figure 7 shows instantaneous vertical profiles of simulated moist static energy, potential temperature and total water, water vapor and liquid water mixing ratios at 125W-30N. The location selected corresponds to that of the DYCOMS II field study (Stevens *et al*. 2003), which provided observational estimates of those profiles. The profiles in Fig. 7 correspond to July 25 of the first simulated year at three different local times: 06:00 (solid lines), 18:00 (dashed), and next 06:00 (dotted). The moist static energy and total water mixing ratio profiles show that these variables are well mixed in the vertical. This is a reasonable feature for a convectively active PBL and is consistent with the DYCOMS II profiles. The potential temperature increases and water vapor mixing ratio decreases with height above the condensation level, and are nearly constant below that level. The multilayer PBL formulation, therefore, can capture the departure of those variables from well-mixed profiles in the cloud layer, as well as the near-constancy of these quantities in other layers. It should be noted, however, that the daily mean liquid-water content simulated by the model appears higher than the DYCOMS II observation. This is another issue that we will address in our future revisions.

The simulated diurnal variation of stratocumulus properties is weaker than the observed (e.g. Duynkerke and Hignett 1993). This is partially due to the missing link between the shortwave radiation, entrainment and TKE in the current formulation, which will be further discussed in Section 7. Thus, the depth of cloud-topped PBL does not show a visible diurnal variation. Nevertheless, there is a clear diurnal variation in temperature and, consequently, in cloud base height since the solar shortwave radiation warms the cloud air in the daytime.

c. Behavior of PBL over Land

In this subsection, we focus on January (austral summer) and select two locations over land corresponding to moist and semi-arid soil. On these locations, therefore, we expect the PBL turbulence to be well developed during daytime. Figure 8 shows the mean diurnal change over five Januarys simulated at the location in the Amazon basin (60W-10S) of the PBL depth (a), ground temperature (b), TKE (c), precipitation (d), latent and sensible heat fluxes from the surface (e), and short and long wave radiation fluxes into the surface (f). The precipitation peaks in the early afternoon during the warm season consistently with observations at nearby locations (Machado et al. 2002; Lin et al. 2000; Bastable et al. 1993). The amplitude of the simulated diurnal cycle of ground temperature is about 6 K, which is similar to the one found in the observations of air temperature close to the ground (e.g., Lin et al. 2000; Bastable et al. 1993). The simulated diurnal cycles of latent, sensible heat and radiation fluxes shown in Figs. 8e and f are also comparable with the observations reported by the same authors. We note that the latent heat flux is much stronger than the sensible heat flux. During morning hours, the short wave radiation heating prevails over the cooling by latent heat and long wave flux, causing the ground temperature to rise. During the late afternoon, the cooling effects prevail and temperature decreases. During night hours, the upward long wave radiation and downward sensible heat fluxes tend to balance at the surface.

Figure 9 shows the same composite diurnal cycles as Fig. 8 except for the location in Australia (135^{o}E and 26^{o}S). The amplitudes of the diurnal cycle of PBL depth, ground temperature, TKE and short and long wave radiation fluxes are stronger than at the location in the Amazon basin. Also, sensible heat flux provides a relatively more important contribution to the net. Precipitation in the Australia location is generally much smaller than at the Amazon basin location, with a weak maximum by early morning. The contribution of cumulus convection to the total precipitation is negligible. During the nighttime hours the PBL becomes

very shallow. During the daytime hours, the high sensible heat flux from the ground contributes to increase TKE and, therefore, the PBL depth.

d. Comparison of the AGCM performance with the new and previous PBL parameterizations

To assess the impact of the new scheme, we compare the simulation described in the previous subsection with another that uses the previous version of the PBL parameterization (hereafter SP simulation). The reader is referred to Suarez *et al*. (1983) for a detailed description of that previous version. In short, the previous parameterization treats the PBL as a well-mixed single layer, the entrainment rate is determined by solving an implicit equation, and the aerodynamic formulas to determine the surface fluxes use mean PBL wind as velocity scale. The implicit equation that determines the entrainment rate is obtained by neglecting the time derivative term in a TKE budget equation similar to (2). A complex iteration procedure discussed by Suarez *et al.* (1983) is used to solve the resulting equation for the entrainment rate. This parameterization has two potential shortcomings in comparison to the new parameterization, first of which is that neglecting the time derivative of TKE in the TKE budget eliminates the transient behavior of PBL. The second is that there is no room to directly implement physical processes for entrainment beyond the equilibrium of TKE.

Figure 10 shows the January- and July-mean PBL depth (a and b, respectively) and stratocumulus incident (c and d, respectively) in the SP simulation. A comparison with Control (Fig. 4) shows that the new parameterization generates more detailed PBL depth patterns (Fig 4a for January and g for July) and a better seasonal variability of stratocumulus incidence (Fig. 4c for January and i for July), particularly in the stratocumulus regions. Fig. 11 shows the January- and July-mean net latent heat fluxes at the surface in SP simulation. Overall, upward fluxes in SP simulation are larger than in the observation (Fig. 5a for January and c for July)

and Control (Fig. 5b for January and d for July). The overall pattern of the fluxes in the southern Tropics in July is less zonal than the observation and Control. Over the eastern Pacific, however, the new formulation gives higher values than the observation and SP simulation. The monthly-mean net shortwave radiation fluxes at the surface for the same months in the SP simulation (Fig. 12a and b) compares reasonably well with both the observed (Fig. 6a and c) and Control (Fig. 6b and d). There is, nevertheless, a small improvement with the new parameterization over the Southern Hemisphere Atlantic and Pacific Oceans in January. It is clear from these comparisons that the new PBL parameterization has overall significantly improved the estimation of the surface latent heat flux in our GCM. Moderate to small improvements are also achieved in the simulation of seasonal variability of stratocumulus incidence and the estimates of net shortwave radiation flux at the surface. We attribute a large part of these improvements to the explicit prediction of TKE and its use in the determination of entrainment rate and surface fluxes in the new PBL parameterization. The overall improvement of the simulated surface latent heat fluxes with the new parameterization is primarily due to the use of the square root of TKE as a velocity scale in the aerodynamical formula for the surface flux. Particularly in the Tropics, where the mean PBL wind is weak, the surface fluxes are controlled by the subgrid scale convective activity, which is well represented by the bulk TKE.

e. Comparison of simulated baroclinic activity with multi- and single-layer PBL parameterizations

In the introduction we stated that explicit prediction of vertical shears within the PBL could have an impact on the evolution of extratropical baroclinic disturbances. To examine this potential impact we select the poleward heat transport near the surface (i.e., within the PBL) in synoptic time scales as a proxy for baroclinic eddy activity. Then, we compare the values for our baroclinic activity to the one obtained by a version of the same AGCM, in which the

number of layers for the PBL is set to one. Otherwise, these two versions of the model are identical.

Figure 13 shows the mean January (upper panel, a and b) and July (lower panel, c and d) latitudinal poleward potential temperature flux by eddies ($v'\theta'$) within the PBL, where prime indicates deviation from the zonal mean, from the CONTROL (left column) and the single-layer simulation (right column). (The values for the CONTROL correspond to vertical averages within the PBL.) To focus on the synoptic scale baroclinic activity, a band-pass filter between 3 and 8 days is applied. A comparison of the panels (a) and (c) to (b) and (d) of Fig. 13, respectively, indicates that the multi-layer scheme generally yields higher baroclinic activity implied by the magnitude of ($v'\theta'$) than the single-layer scheme does. It should be noted that the horizontal resolutions we are using are insufficient to properly resolve the details of synoptic scale eddies. Nevertheless, our comparison still indicates that the use of multiple layers in the PBL produces a more realistic level of baroclinic activity.

f. Performance of the AGCM coupled to an OGCM

We have also performed simulations in which the AGCM coupled to a near global MIT-OGCM. [The reader is referred to Cazes-Boezio *et al*. (2005) for the coupled model results.] Experiments in the coupled mode is a necessary task to validate AGCMs since prescribing SSTs in the uncoupled mode assumes the most important part of the answer and, therefore, it may hide crucial deficiencies of the model.

In the coupled simulations, the SST field (not shown) demonstrates several realistic features both in terms of annual means (such as realistic equatorial SST gradients in both Pacific and Atlantic basins) and interannual variability (such as ENSO-like anomalies in SST and the atmospheric circulation). The outstandingly successful feature of the simulations is that

the extent and seasonal cycle of stratocumulus clouds and their effects on short wave radiation and SST in the eastern part of the subtropical oceans are well simulated. We attribute a large part of this success to the merits of our PBL framework.

4. Importance of interactions between radiation and turbulence in a cloud-topped PBL

In this section we examine the importance of radiation, turbulence and thermodynamics interactions in the PBL when stratocumulus clouds are present. The radiative cooling at the PBL top is of fundamental importance for the generation of TKE and turbulence fluxes in a cloud-topped PBL. In the formulation we are presenting here, the PBL top coincides with that of stratocumulus clouds. Hence, the radiation calculation in the AGCM directly gives the value of radiative cooling at the PBL top, which is then explicitly included in the formulations of the TKE generation, PBL-top mass entrainment, and the time derivative of potential temperature of the uppermost PBL layer. In our model, therefore, the importance of this cooling can easily be assessed by an experiment in which this effect is neglected.

We focus on July, during which the high incidence of stratocumulus in the eastern parts of tropical and subtropical oceans is generally well captured by the AGCM (see Fig. 2). We start by performing a simulation in which radiative cooling at the PBL top is set to zero in the calculation of TKE and mass entrainment, but kept in the potential temperature prediction (hereafter "NR1 simulation"). Note that the radiative cooling affects the TKE budget through the buoyancy generation as discussed in subsection 2*b* (i). The impact of its overall effect can be seen in the differences between the NR simulation and that presented in Section 3 (hereafter "Control"). Figure 14 shows TKE, PBL depth and stratocumulus incidence from the NR1 simulation (Fig. 14a, c and e, respectively) and the differences from the Control (NR1 simulation–Control) (Figs. 4h, g and i). In the eastern parts of the subtropical and tropical

oceans, regions in which stratocumulus incidence obtained in the Control is high, the PBL depth, TKE and stratocumulus incidence are reduced in the NR1 simulation. Off the coast of California, the reduction is as high as 60%, while off the coasts of Peru and Namibia the reduction is about 30%. The lack of radiative cooling effect at the PBL reduces the TKE and entrainment rate in the stratocumulus region, and thus the PBL becomes shallower. A positive feedback is established as the PBL top lowers and condensation level rises. Along the North Pacific storm track, both the NR1 simulations and Control show a very shallow PBL (Figs. 4g and 14c), low TKE, and high stratocumulus incidence (Figs. 4i and 13e). In this region, PBL is usually stable. In such a situation, the lower entrainment rate produces higher incidence of fog since the mixing of air between the PBL and the overlying drier free atmosphere is reduced.

Despite the lower incidence of stratocumulus clouds in the eastern parts of subtropical and tropical regions in the NR1 simulation, there are still local maxima of PBL depth in these regions. This is partially due to the TKE generation by the upward surface heat fluxes resulting from low-level cold advection from higher latitudes along the eastern branch of the subtropical anticyclones. In addition, the radiative cooling of the cloud layer is still active in the NR1 simulation.

To completely eliminate the effects of radiative cooling that influences the PBL, we set the radiative cooling to zero both in the calculation of TKE and mass entrainment and in the potential temperature prediction in the uppermost PBL layer. We call this experiment NR2. In this experiment, the stratocumulus incidence for July (see Fig. 15) is further reduced from the NR1 simulation (Fig. 14) to the point of almost vanishing even in the regions where they are most persistent in the Control (Fig. 4).

A comparison of the results of NR1 and NR2 experiments reveals that the cooling of the PBL air due to the cloud-top radiative cooling indirectly contributes to the budget of TKE (and

therefore entrainment rate) and helps, to a certain degree, maintenance of stratocumulus decks over oceans. The indirect link is through the enhanced surface heat fluxes (and, therefore, through the buoyancy contribution to TKE) caused by the cooler PBL air under the clouds. This indicates the existence of a feedback process between the PBL clouds and surface heat fluxes.

5. Comparison with models with the traditional vertical structure

In the previous section, we presented a comparison to assess the effect of processes associated with stratocumulus clouds on the turbulence fluxes using the new framework. To what degree the lack of these processes in a model with a traditional PBL parameterization influences the simulations is an interesting question. There have been many studies that combine a traditional parameterization with interactive cloud parameterizations beyond diagnostic treatments (e.g., Soares *et al*., 2004; Lock *et al*., 2000). In this paper, however, what we mean with the traditional PBL parameterization is a parameterization characterized by two aspects. One is the use of the "traditional" vertical structure, in which the vertical coordinate is a terrain following sigma type. As mentioned earlier, we use a different vertical structure, in which the PBL has its own multiple layers with predicted depth. In an early version of the UCLA GCM, an attempt was made to incorporate a mixed-layer based PBL parameterization, with a traditional vertical structure (Randall, 1976). Not having the PBL top coinciding with a coordinate surface in the traditional vertical structure made the PBL-top jump very difficult to determine and caused the abandonment of this attempt later (Suarez *et al*., 1983). This experience is an indication that the vertical structure we use is paramount for a successful incorporation of the new PBL parameterization to our model. The second aspect of what we mean by the traditional parameterization is the use of diagnostically determined PBL clouds

without formulation of their effects in the parameterization itself. We use such a parameterization to see the difference between prognostic and diagnostic determinations of clouds in a simple context.

How the results obtain by a model with the traditional PBL parameterization compare to those presented in section 3 is examined here. For this purpose we constructed a version of our model with the traditional vertical structure. To do that, first we replace the part of the vertical coordinate given by (1b) and (1c) for $p_I \le p \le p_S$ by a conventional sigma coordinate such as the one defined as $\sigma_{trop} \equiv 2\left(p - p_I\right)/\left(p_S - p_I\right)$. Note that the total number of model layers is kept the same as in the Control. For the PBL parameterization, we choose the scheme used by Holtslag and Boville (1993). The scheme requires a definition of the PBL depth, for which we choose the diagnostic expression using a bulk Richardson number introduced by Troen and Mahrt (1986). In this experiment, we diagnose the PBL depth at each dynamics time step. To diagnose the PBL clouds, we calculated the lifting level of condensation (LLC). If the LLC is below the PBL-top height, it is assumed that the PBL is topped with stratocumulus clouds.

Figure 16 shows the July-mean distribution of the PBL depth, stratocumulus incidence diagnosed for the PBL and low-level cloud incidence simulated by this experiment, which we call the *fixed-sigma* simulation. The low-level cloud incidence (cloud incidence for the lowest 250 mb deep portion of the troposphere) is presented because the stratocumulus clouds incidence diagnosed for the PBL may not fully represent the clouds resulted from the PBL processes in the *fixed-sigma* simulation. In the subtropical oceans, the distributions of maximum and minimum of the PBL depth distribution (Fig. 16a) are almost opposite to those in the Control (Fig. 4g). In the *fixed-sigma* experiment, the regions of the observed high incidence of marine stratocumulus off the coasts of California, Peru and Namibia show relative *minima* of

PBL depth while those in the western parts of the oceans show relative *maxima*. Altogether, the patterns in Fig. 16a are very unrealistic. The incidence of stratocumulus clouds tends to have relative *maxima* in the western parts of the oceans in the *fixed-sigma* experiment while relative *maxima* appear in the eastern parts of the oceans in the Control. The stratocumulus incidence in the low-pressure belt around Antarctica is relatively well simulated, but it has a more zonal pattern than in the Control. The low-level cloud incidence for July shown in Fig. 16c is overall unrealistically high almost everywhere, and tends to have relative *minima* in the usual marine stratocumulus regions.

We interpret the differences between the results presented in Fig. 16 and the Control as the results of two main deficiencies in the *fixed-sigma* model. First, the formula that determines the PBL depth is diagnostic without considering the mass budget. Second, the processes at the cloud top that influence the turbulent fluxes are absent. According to the diagnostic equation that determines the PBL depth in the *fixed-sigma* model, the surface heat flux and the mean shear are the two main controllers of the PBL depth (The higher the upward flux is and/or the stronger the shear is, the deeper the PBL is.) In the *fixed-sigma* simulation, therefore, the PBL tends to be deeper in the areas with high SSTs. Only when the PBL is deep enough, the stratocumulus clouds can be maintained regardless of the processes associated with these clouds. In this sense, it is not surprising that the important features of the marine PBL are poorly simulated in the *fixed-sigma* experiment.

6. Summary and Discussions

In this paper, we present the basic features and an assessment of a newly developed PBL parameterization scheme implemented in the UCLA AGCM. The new scheme maintains many features of the previous PBL schemes of the UCLA AGCM (Suarez *et al*. 1983). These

features can be summarized as follows: the depth of PBL is predicted through the mass budget for the PBL including the entrainment through its top, the cumulus mass flux and the vertically integrated horizontal mass flux convergence. Within the PBL a modified sigma coordinate is used, in which the PBL and free atmosphere share a coordinate surface at the PBL top. The PBL top then becomes a material surface in the absence of entrainment (or detrainment) and cumulus mass flux. The new PBL scheme uses multiple layers within the PBL as opposed to the single layer in the previous schemes. The vertically integrated turbulence kinetic energy (TKE) is predicted through a kinetic energy budget equation including the buoyancy and shear generation, dilution due to the PBL-top mass entrainment, and dissipation. The buoyancy generation includes the effects of the upward surface heat fluxes and radiative cooling at the cloud top (PBL-top and cloud top coincide if the PBL is cloudy). The PBL top entrainment is determined from a formulation that takes into account the effects of TKE and the radiative and evaporative cooling concentrated near the PBL top (Randall and Schubert 2004). The surface fluxes are determined from an aerodynamic formula, in which a combination of the square root of TKE and the grid-scale surface wind are used to represent the velocity scale. The turbulent fluxes within the PBL are determined through an approach considering the effects of both large convective and small diffusive eddies through bulk and K-closure formulations, respectively. Using these fluxes, we explicitly predict the vertical profiles of the variables.

To illustrate the performance of the model with the new PBL parameterization, we carried out simulations in an uncoupled mode with prescribed SST and in a coupled mode using a near global MIT-OGCM. In this paper, we present the results from the uncoupled simulations. Monthly-mean fields of the simulated SLP, PBL height, TKE, stratocumulus incidence, and net solar radiation and latent heat fluxes at the surface are shown. These fields (except PBL height and TKE, for which observations are not available) match reasonably well

to their observed counterparts. The distribution and seasonal variation of the stratocumulus incidence off the coasts of California, Peru and Namibia are realistic. A comparison of these results to the ones obtained by using the previous version of the PBL parameterization demonstrates an overall improvement in the simulations with the new parameterization. The simulated PBL profiles near the location of DYCOMS II field experiment demonstrate the same major features of the observed profiles. The composite diurnal cycles of various fields including PBL depth and precipitation over moist and semi-arid land points are also examined. Over a semi-arid land point, the PBL reaches its maximum depth late afternoon just before sunset and crashes rapidly after sunset completing a cycle as observed in nature. Over moist land (a point chosen in the Amazon region), the diurnal cycle of precipitation shows precipitation peaks in the afternoon as observed.

Simulation of the formation and maintenance of the marine stratocumulus decks off the coasts of California, Peru and Namibia presents a real challenge for climate models. Success of the model generally depends on the formulation of the interactions between radiation, turbulence and thermodynamics in the cloud-topped PBL. While the results presented in section 3 confirm the overall effectiveness and realism of the parameterized PBL processes with the new formulation, we additionally performed experiments to demonstrate the important role of these interactions in maintaining marine stratocumulus decks. We first eliminated the turbulence and radiative cooling interaction by setting the radiative cooling to zero in the buoyancy generation of TKE and in the entrainment formula. The results obtained from this experiment are very different from those of the control simulation. In the usual stratocumulus regions, the simulated cloud incidence is drastically reduced and the PBL becomes shallower and less turbulent compared to the Control. As an extension of this experiment, the radiative cooling effect is also removed from the potential temperature equation for the uppermost PBL

layer. The simulation from this experiment virtually eliminates already infrequent stratocumulus incidence. These two experiments indicate that it is very difficult to maintain the clouds against the destructive effects of subsidence prevailing in these regions without properly simulating the cloud radiative cooling, turbulence and temperature interactions.

We also examine whether the AGCM would yield very different results if a PBL parameterization based on the formulation described by Holtslag and Boville (1993) is used. For this purpose, we modify the model to use the conventional sigma coordinate and determine the PBL height using the formula introduced by Troen and Mahrt (1986) and used by Holtslag and Boville (1993). The results are significantly worse than the Control particularly for the stratocumulus incidence over the oceans. This comparison also confirms the importance of cloud radiation-turbulence interaction processes in the PBL parameterization for realistic simulations of the stratocumulus clouds.

In the coupled simulations (not shown here), the SST field illustrates realistic equatorial SST gradients in both Pacific and Atlantic basins both in terms of annual means and interannual variability (such as ENSO-like anomalies in SST and the atmospheric circulation). We attribute a large part of this success to the merits of the PBL framework we used, particularly those involved in realistic representation of physical processes associated with stratocumulus.

Two issues remain, one of which is related to the transparency of the stratocumulus clouds and the other related to the higher than observed liquid-water content in the stratocumulus decks, as discussed in subsections *3a* and *3b*, respectively. Both issues are complex and will be addressed in the future model revisions. The first step in this direction should be a detailed examination of simulated diurnal and seasonal variations of liquid water path with the current model. An observational analysis of diurnal and seasonal variations of liquid water path is presented by Wood *et al.* (2002).

One of the main weaknesses of existing AGCMs, including the model presented here, is poor representation of interactions between PBL and cumulus convection. The use of multiple layers within the PBL is the first step in our plan improving the simulation of these interactions. Another common weakness of AGCMs is in the simulation the stably stratified PBL regimes (Holtslag 2003; Derbyshire 1990; and Beljaar and Holtslag 1991). An excellent discussion on this subject can be found in Mahrt (1999). Since the PBL reduces to a shallow layer for this condition, which is not well mixed, our new multi-layer framework should provide the necessary structure to treat the stable shallow layer. Yet, a proper parameterization of physical processes involved in a stable PBL remains to be decided.

This paper presents a preliminary assessment of a new multi-layer framework for parameterizing PBL processes. So far, it is shown that the multi-layer framework is advantageous for more realistic simulations of baroclinic activity compared to the single-layer framework. Yet, much more work is needed to fully benefit from its potential, such as predicting the TKE for each PBL layer and inclusion of a scheme to represent the cumulus roots. Bechtold *et al*. (1992) presents a PBL parameterization, in which the vertical transport of TKE is formulated through a diffusive flux. However, TKE is in our model is for large-eddies so that the transport may not be diffusive. It is one of our goals to improve this aspect of Bechtold *et al*. model to implement our model to predict TKE for each layer. To design a scheme for cumulus roots, we may take advantage of very high-resolution cloud resolving model simulations.

Acknowledgements. Professor David Randall and his colleagues at Colorado State University carried out the basic work on the bulk parameterization. This project was funded by U.S. DOE under grant numbers DE-FG02-04ER63848, DE-FG02-02ER63370 and DE-FC02-06ER64302

to Colorado State University, CSU Contracts G-3816-3 and G-3818-1 to UCLA, and NSF under grant number ATM-0415184 to Colorado State University.

References

Arakawa, A., 2004: The Cumulus Parameterization Problem: Past, Present, and Future**.** *J. Climate*, **17**, 2493–2525.

Arakawa, A., and V. R. Lamb, 1977: Computational design of the basic dynamical process of the UCLA general circulation model. *Methods in Computational Physics*, **17**, Academic Press, 173-265.

Arakawa, A., and M.J. Suarez, 1983: Vertical differencing of the primitive equations in sigma-coordinates. *Mon. Wea. Rev.*, **111**, 34-45.

Arakawa, A., and W. H. Schubert, 1974: Interaction of a cumulus cloud ensemble with the large-scale environment, Part I. *J. Atmos. Sci.*, **31**, 674-701.

Bastable, H. G., W. J. Shuttleworth, R. L. G. Dallarosa, G. Fisch and C. A. Nobre, 1993: Observations of Climate, albedo, and surface radiation over cleared and undisturbed Amazonian forest. *Int. J. Climatol.*, **13**, 783-796.

Bechtold, P., C. Fravalo and J. P. Pinty, 1992: A model of marine boundary-layer cloudiness for mesoscale applications. *J. Atmos. Sci.*, **49**, 1723-1744.

Beljaars, A. C. M., and A. A. M. Holtslag, 1991: Flux parameterization and land surfaces in atmospheric models. *J. Appl. Meteor*. **30**, 327-341.

Boville, B. A., 1991: Sensitivity of simulated climate to model resolution. *J. Climate*, **4**, 469-485.

Breidenthal, R. E. and M. B. Baker, 1985: Convection and entrainment across stratified interfaces. *J. Geophys. Res.*, **90D**, 13055-13062.

Breidenthal, R. E., 1992: Entrainment at thin stratified interfaces: The effects of Smith, Richardson and Reynolds numbers. *Phys. Fluids A*, **4**, 2141-2144.

Bretherton, C. S., [and list of authors] 2004: The EPIC 2001 Stratocumulus study. *Bull. Am. Met. Soc.*, **85**, 967-977.

Cazes Boezio, G., C. S. Konor, A. Arakawa, C. R. Mechoso, and D. Menemenlis, 2005: Coupled simulations obtained with the UCLA AGCM with a new PBL parameterization and the MIT global OGCM. Proceedings of the 17h Conference on Climate Variability of the American Meteorological Society, Cambridge, Massachusetts, May 2005.

Da Silva, A. C. Young, and S. Levitus, 1994: Atlas of surface marine data, volume 1: Algorithms and procedures. *Tech. Rep. 6, U.S. Department of Commerce, NOAA, NESDIS, 1994.*

Deardorff, J. W., 1972: Parameterization of the planetary boundary layer use in general circulation models. *Mon. Wea. Rev*, 93-106.

Deardorff, J. W., 1980: Cloud top entrainment instability. *J. Atmos. Sci*, **37**, 329-350.

Del Genio, A., M.-S. Yao, W. Kovari, and K. K.-W. Lo:, 1996: A prognostic cloud water parameterization for global climate models. *J. Climate*, **9**, 270-304.

Derbyshire, S. H., 1990: Boundary-layer decoupling over cold surfaces as a physical boundary-instability. *Boundary-Layer Meteorol*. **82**, 297-325.

Dorman, J. L., and P. J. Sellers, 1989: A global climatology of albedo, roughness length and stomatal resistance for atmospheric general circulation models as represented by the Simple Biosphere model (SiB). *J. Appl. Meteor.*, **28**, 833-855.

Duynkerke, P. G., and P. Hignett, 1993: Simulation of diurnal variation in a stratocumulus-capped marine boundary layer during FIRE. *Mon. Wea. Rev.*, **121**, 3291-3300.

Grenier H., and C. S. Bretherton, 2001: A Moist PBL Parameterization for Large-Scale Models and Its Application to Subtropical Cloud-Topped Marine Boundary Layers. *Mon. Wea. Rev*., **129**, 357-377.

Harshvardhan, R D., D. A. Randall, and T. G. Corsetti, 1987: A fast radiation parameterization for atmospheric circulation models. *J. Geophys. Res.*, **92**, 1009-1016.

Harshvardhan, R. D, D. A. Randall, T. G. Corsetti, and D. A. Dazlich, 1989: Earth radiation budget and cloudiness simulations with a general circulation model. *J. Atmos. Sci.*, **46,** 1922–1942.

Holtslag A. A. M., 2003: GABLS initiates intercomparison for stable boundary layer case. *GEWEX Newsletter*, **13**, No 2 (May), 7-8.

Holtslag A. A. M., and B. A. Boville, 1993: Local versus nonlocal Boundary-layer diffusion in a global model. *J. Climate*, **6**, 1825-1842.

Kalnay. E., [and list of authors] 1996: The NCEP/NCAR 40-Year Reanalysis project. *Bull. Am. Met. Soc.*, **77**, 437-471.

Klein S. A., and D. L. Hartmann, 1993: The seasonal cycle of low stratiform clouds. *J. Climate*, **6**, 1587-1606.

Konor C. S., and A. Arakawa, 2005: Incorporation of moist processes and a PBL parameterization into the generalized vertical coordinate model. Technical Report No 765, Department of Atmospheric Science, Colorado State University, 75 pp. Available from http://kiwi.atmos.colostate.edu/pubs/PBL_tech_report_CSU_2005.pdf.

Konor C. S., and A. Arakawa, 2008: Incorporation of a PBL parameterization into a general circulation model. Updated technical report No 765, Department of Atmospheric Science, Colorado State University, 70 pp. Available from http://kiwi.atmos.colostate.edu/pubs/New_PBL_Tech_Rep_sigma_GCM.pdf.

Konor, C. S., G. Cazes Boezio, C. R. Mechoso, and A. Arakawa, 2004: Evaluation of a new PBL paramaterization with emphasis in Surface Fluxes. Proceedings of the 13th Conference on Interactions of the Sea and Atmosphere of the American Meterological Society, (edited as CD), paper 2.11, Portland, Maine, 9-13 August 2004.

Krasner, R. D., 1993: Further Development and Testing of a Second-Order Bulk Boundary Layer Model. M.S. Thesis, Department of Atmospheric Science, Colorado State University. 131 pp.

LeTreut, H., and Z.-H. Li, 1991: Sensitivity of an atmospheric general circulation model to prescribed SST changes: Feedback effects associated with the simulation of cloud optical properties. *Climate Dyn.*, **5**, 175-187.

Lilly, D. K., 1968: Models of cloud-topped mixed layers under a strong inversion. *Quart. J. Roy. Meteor. Soc.*, **94**, 292-309.

Lilly, D. K., 2002: Entrainment into mixed layers. Part I: a new closure. *J. Atmos. Sci*, **59**, 3353-3361.

Lin, X., D. A. Randall and L. D. Fowler, 2000: Diurnal variability of the hydrologic cycle and radiative fluxes: comparisons between observations and a GCM. *J. Climate*, **13**, 4159-4179.

Lock A. P., A. R. Brown, M. R. Bush, G. M. Martin, and R. N. B. Smith, 2000: A new boundary layer mixing scheme. Part I: Scheme description and single-column Model. *Mon. Wea. Rev.*, **128**, 3187-3199.

Lock A. P., 1998: The Parameterization of entrainment in cloudy boundary layers. *Quart. J. Roy. Meteor. Soc.*, **124**, 2729-2753.

Louis, J. F., 1979: A parametric model of vertical eddy fluxes in the atmosphere. *Boun.-Layer Meteor.*, **17**, 187-202.

Louis, J. F., M. Tiedke, and J. F. Geleyn, 1982: A short history of the PBL parameterization at ECMWF. *Proc. ECMWF Workshop on Boundary-Layer Parameterization*, ECMWF 59-79 [Available from ECMWF, Shinfield Park, Reading RG2 9AX U.K.]

Ma, C. -C., C. R. Mechoso, A. W. Robertson, and A. Arakawa, 1996: Peruvian Stratus Clouds and the Tropical Pacific Circulation: A Coupled Ocean-Atmosphere GCM Study, *J. Climate*, **9**, 1635-1645.

Machado, L. A. T., H. Laurent, and A. A. Lima, 2002: Diurnal march of the convection observed during TRMM-WETAMC/LBA, *J. Geophys. Res.*, **107** (D20), 8064-8077.

Mahrt, L., 1999: Stratified atmospheric boundary layers. *Boundary-Layer Meteorol*. **90**, 375-396.

Martin G. M., M. R. Bush, A. R. Brown, Lock A. P., and R. N. B. Smith, 2000: A new boundary layer mixing scheme. Part II: Tests in climate and mesoscale models. *Mon. Wea. Rev.*, **128**, 3200-3217.

Mechoso, C.R., J-Y. Yu, and A. Arakawa, 2000: A coupled GCM pilgrimage: from climate catastrophe to ENSO simulations. General Circulation Model Development: Past, Present and Future. Proceedings of a Symposium in Honor of Professor Akio Arakawa, D. A. Randall, Ed., Academic Press, pp. 539-575.

Mellor G. L., and T. Yamada, 1982: Development of a turbulence closure model for geophysical fluid problems. *Rev. Geophys. Space Phys.,* **20**, 851-875.

Moeng, C.-H., 2000: Entrainment rate, cloud fraction and liquid water path of PBL stratocumulus clouds. *J. Atmos. Sci*, **57**, 3627-3643.

Moeng, C. –H., and P. P. Sullivan, 1994: A comparison of shear- and buoyancy-driven planetary boundary layer flows. *J. Atmos. Sci.,* **51**, 999-1022.

Pan, D. M., and D. A. Randall, 1998: A cumulus parameterization with a prognostic closure. *Quart. J. Roy. Meteor. Soc.*, **124**, 949-981.

Randall, D. A., 1976: The interaction of the planetary boundary layer with large scale circulations. Ph. D. Thesis, The University of California. Los Angeles, 247 pp.

Randall, D. A., 1980a: Conditional instability of the first kind upside-down. *J. Atmos. Sci.*, **37**, 125-130.

Randall, D. A., 1980b: Entrainment into a stratocumulus layer with disturbed radiative cooling. *J. Atmos. Sci*., **37**, 148-159.

Randall, D. A., R. D. Harshvardhan, D. A. Dazlich, and T. G. Corsetti, 1989: Interactions among Radiation, Convective, and Large-Scale Dynamics in a General Circulation Model, *J. Atmos. Sci*, **46**, 1943-1970.

Randall, D. A., Q. Shao, and C. –H. Moeng, 1992: A second-order bulk boundary layer model. *J. Atmos. Sci.*, **49**, 1903-1923.

Randall D. A., and W. H. Schubert, 2004: Dreams of a stratocumulus sleeper. In Atmospheric Turbulence and Mesoscale Meteorology, Scientific Research Inspired by Doug Lily, E. Fedorovich, R. Rotuno and B. Stevens (eds.), Cambridge University Press, 95-114.

Rayner, N. A., C. K. Folland, D. E. Parker, and E. B. Horton, 1995:A new global sea-ice and sea surface temperature (GISST) data set for 1903–1994 for forcing climate models. Hadley Centre Internal Note 69, U.K. Met. Office, 14 pp.

Siems, S. T., C. S. Bretherton, M. B. Baker S. Shy, and R. E. Breidenthal, 1990: Buoyancy reversal and cloud top instability. *Quart. J. Roy. Meteor. Soc.*, **116**, 705-739.

Slingo, A. S., Nicholls, and J. Schmetz, 1982: Aircraft observations of marine stratocumulus during JASIN, *Quart. J. Roy. Meteor. Soc.,* **108**, 833-856.

Smith, R. N. B., 1990: A scheme for predicting layer clouds and their water content in a general circulation model. *Quart. J. Roy. Meteor. Soc.,* **116**, 435-460.

Soares, P. M. M., P. M. A. Miranda, A. P. Siebesma, and J. Teixeira, 2004: An eddy-diffusivity/mass-flux parameterization for dry and shallow cumulus convection. *Quart. J. Roy. Meteor. Soc.,* **130**, 3365-3383.

Stevens, B., 2002: Entrainment in stratocumulus topped mixed layers, *Quart. J. Roy. Meteor. Soc.*, **119**, 2663-2689.

Stevens, B., [and list of authors] 2003: Dynamics and Chemistry of Marine Stratocumulus, DYCOMS-II, *Bull. Am. Met. Soc.*, **84**, 1579-593.

Suarez, M. J., A. Arakawa, and D. A. Randall, 1983: The parameterization of the planetary boundary layer in the UCLA general circulation model: Formulation and results. *Mon. Wea. Rev.*, **111**, 2224-2243.

Sundqvist, H., 1978: A parameterization scheme for non-convective condensation including prediction of cloud water content, *Quart. J. Roy. Meteor. Soc.*, **104**, 677-690.

Terra, R., 2004: PBL stratiform cloud inhomogeneities thermally induced by the orography: a parameterization for climate models. *J. Atmos. Sci.*, **61**, 644–663

Tokioka, T., K. Yamazaki, I. Yagai, and A. Kitoh, 1984: A description of the Meteorological Research Institute atmospheric general circulation model (MRI GCM-I). MRI Tech. Report No. 13, Meteorological Research Institute, Ibaraki-ken, Japan, 249 pp.

Troen, I., and L. Mahrt, 1986: A simple model of the atmospheric boundary layer: Sensitivity to surface evaporation. *Boun.-Layer Meteor.,* **37**, 129-148.

Turton, J. D., and S. Nicholls, 1987: A study of the diurnal variations of stratocumulus using a multiple mixed layer model. *Quart. J. Roy. Meteor. Soc.,* **113**, 969-10.

Wood, R., C. S. Bretherton, and D. L. Hartmann, 2002: Diurnal cycle of liquid water path over the subtropical and tropical oceans. *Geophys. Res. Lett*. 10.1029/2002GL015371.

Zhang, C., D. A. Randall, C. –H. Moeng, M. Branson, K. A. Moyer, and Q. Wang, 1996: A surface flux parameterization based on the vertically averaged turbulence kinetic energy. *Mon. Wea. Rev* ., **124**, 2521-2536.

Figure Captions

FIG. 1. A Schematic depiction of the vertical structure of the PBL with the new scheme.

FIG. 2. Vertical structure and sigma coordinate of the UCLA-AGCM.

FIG. 3. Sea level pressure (hPa, SLP) from NCEP reanalysis (left column) and simulations (right column) for January (upper row) and July (lower row).

FIG. 4. Monthly-mean PBL-depth (hPa, with 30 hPa contour interval, left column), TKE (m^2s^{-2}, with 0.2 m^2s^{-2} contour intervals, middle column) and stratocumulus incidence (with 0.2 contour interval, right column) for January (uppermost row), April (second from top), July (third from top) and October (lowermost row).

FIG. 5. Latent heat flux (Wm^{-2}) at the surface from the COADS analysis (left column) and simulations (right column) for January (upper row) and July (lower row). Upward flux is positive with 30 Wm^{-2} contour intervals.

FIG. 6. Net short wave radiation flux (Wm^{-2}) at the surface from the NASA SRB analysis (left column) and simulations (right column) for January (upper row) and July (lower row). Downward flux is positive with 30 Wm^{-2} contour intervals.

FIG. 7. Vertical profiles of moist static energy (left), potential temperature (second from left), total water mixing ratio (middle), water vapor mixing ratio (second from right) and liquid water mixing ratio (right).

FIG. 8. Mean diurnal cycles at 60W-10S for January of (a) PBL thickness, (b) ground temperature, (c) TKE, (d) hourly precipitation rate, (e) upward latent and sensible heat flux at Earth's surface (curves indicated with "LH" and "SH", respectively) and (f) downward short and long wave radiation fluxes at Earth's surface (the curves indicated

with “SW” and “LW”, respectively). The diurnal cycles are given as function of local time.

FIG. 9. Same as Fig. 8, except at 135W-26S.

FIG. 10. Same as relevant panels of Fig.4, except for the SP simulation.

FIG. 11. Same as Fig.5, except for the SP simulation.

FIG. 12. Same as Fig.6, except for the SP simulation.

FIG. 13. Monthly-mean longitudinal potential temperature flux by eddies (^{o}Kmsec^{-1}). Upper and lower panels are for January and July, respectively. Left and right columns show results from the multi-layer CONTROL and single-layer simulation, respectively.

FIG. 14. Monthly-mean TKE (upper panel), PBL thickness (hPa, middle panel) and stratus incidence (lower panel) from the simulation with no radiative cooling effect in TKE and entrainment (NR1, left column) and difference between NR1 and Control (Fig. 4) simulations (right column).

FIG. 15. Monthly-mean stratocumulus incidence from the simulation with no radiative cooling effect on TKE, entrainment and potential temperature for July (NR2 experiment).

FIG. 16. (a) Monthly-mean PBL depth (hPa), (b) stratocumulus incidence (within the PBL) and (c) low-level cloud incidence (cloud incidence for the lowest 250 mb deep portion of the troposphere) for July from *fixed-sigma* simulation. See Fig. 4 for contour intervals.

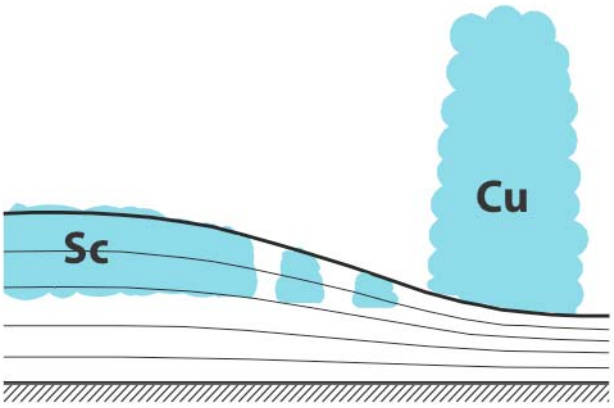

FIG. 1. A Schematic depiction of the vertical structure of the PBL with the new scheme.

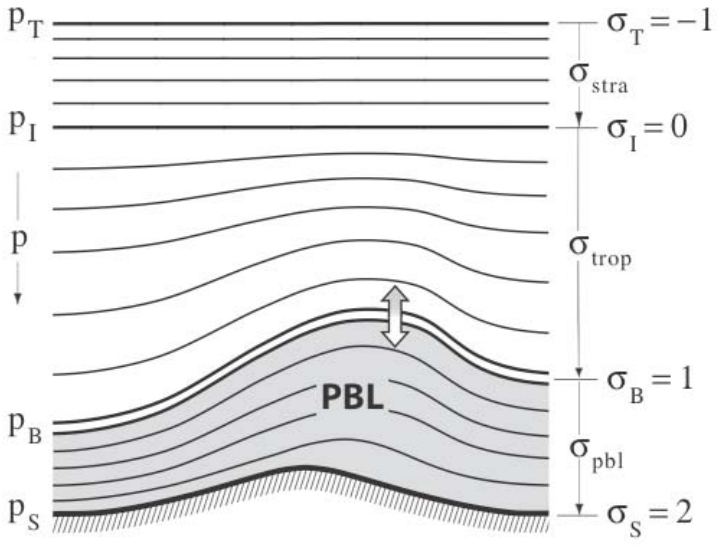

FIG. 2. Vertical structure and sigma coordinate of the UCLA-AGCM.

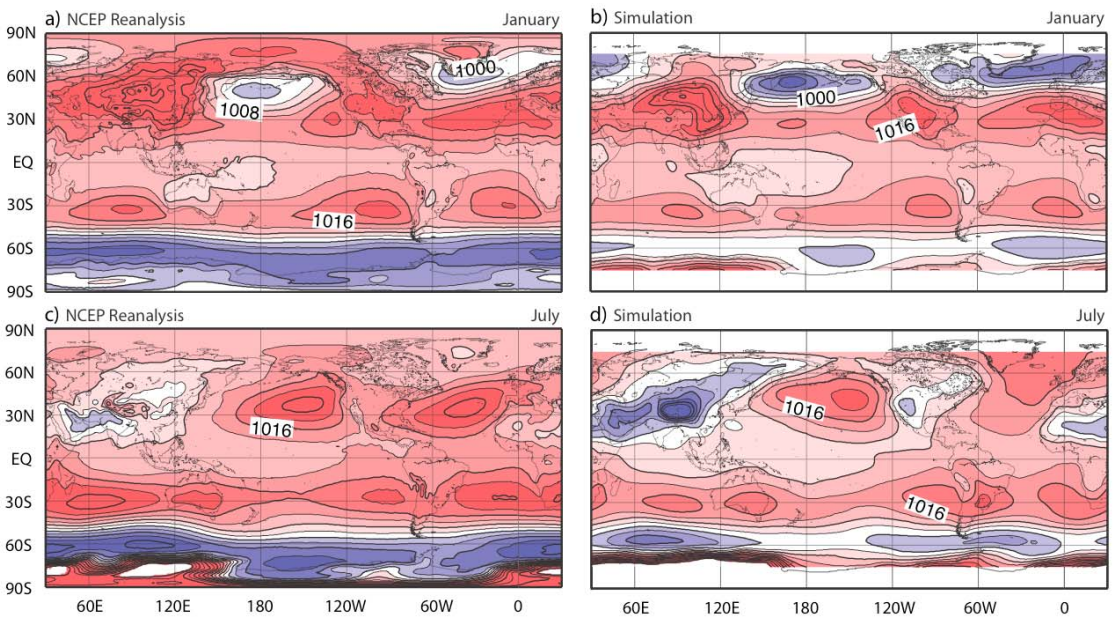

FIG. 3. Sea level pressure (hPa, SLP) from NCEP reanalysis (left column) and simulations (right column) for January (upper row) and July (lower row).

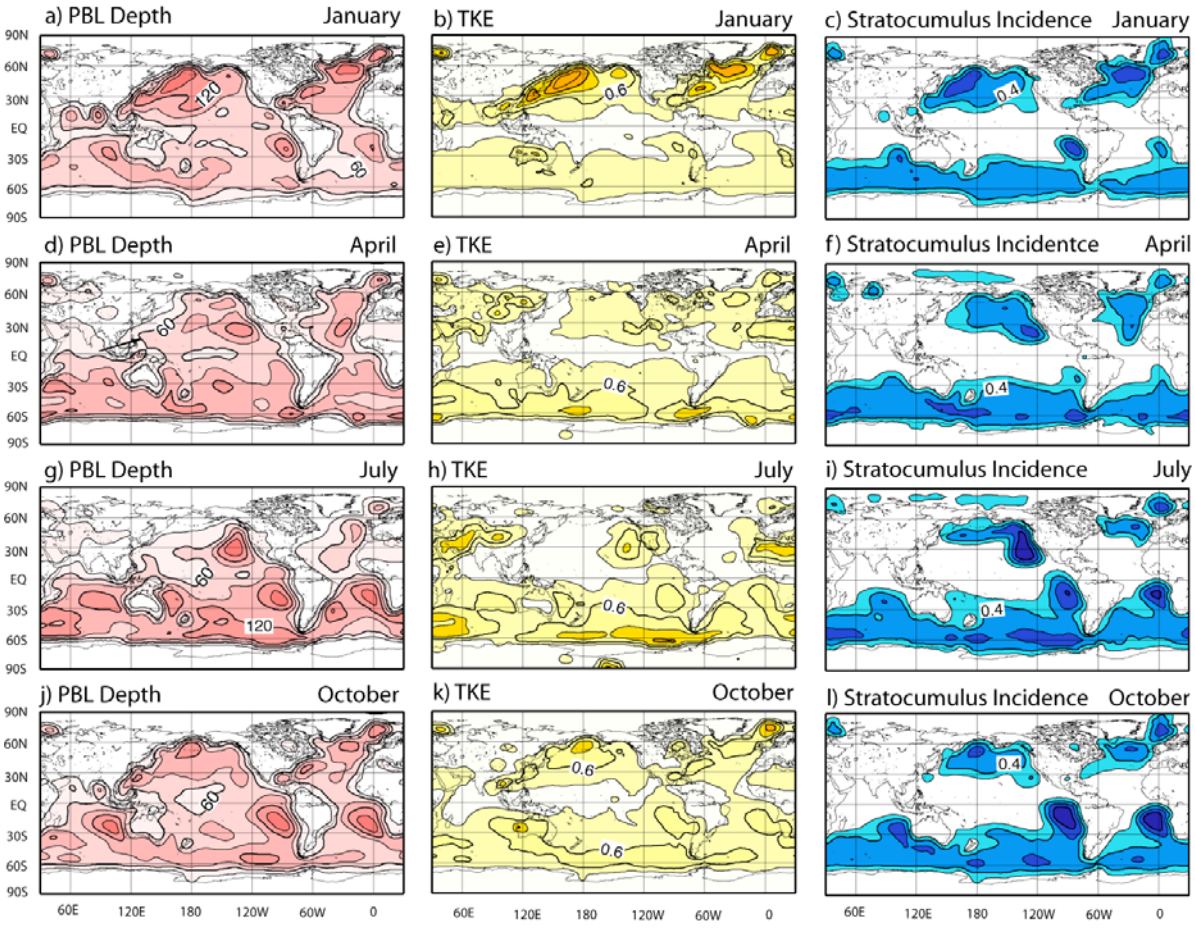

FIG. 4. Monthly-mean PBL-depth (hPa, with 30 hPa contour interval, left column), TKE (m^2s^{-2}, with 0.2 m^2s^{-2} contour intervals, middle column) and stratocumulus incidence (with 0.2 contour interval, right column) for January (uppermost row), April (second from top), July (third from top) and October (lowermost row).

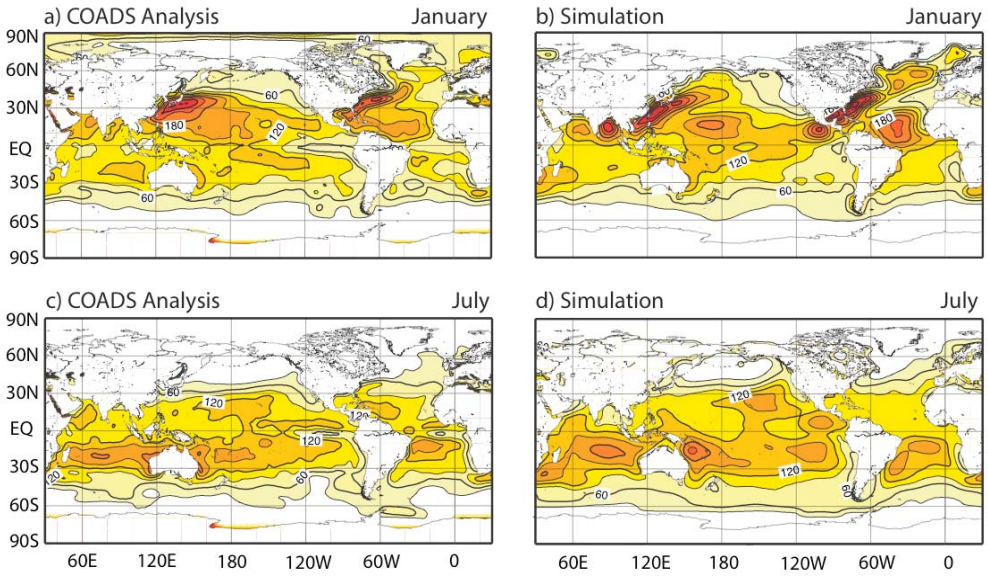

FIG. 5. Latent heat flux (Wm^{-2}) at the surface from the COADS analysis (left column) and simulations (right column) for January (upper row) and July (lower row). Upward flux is positive with 30 Wm^{-2} contour intervals.

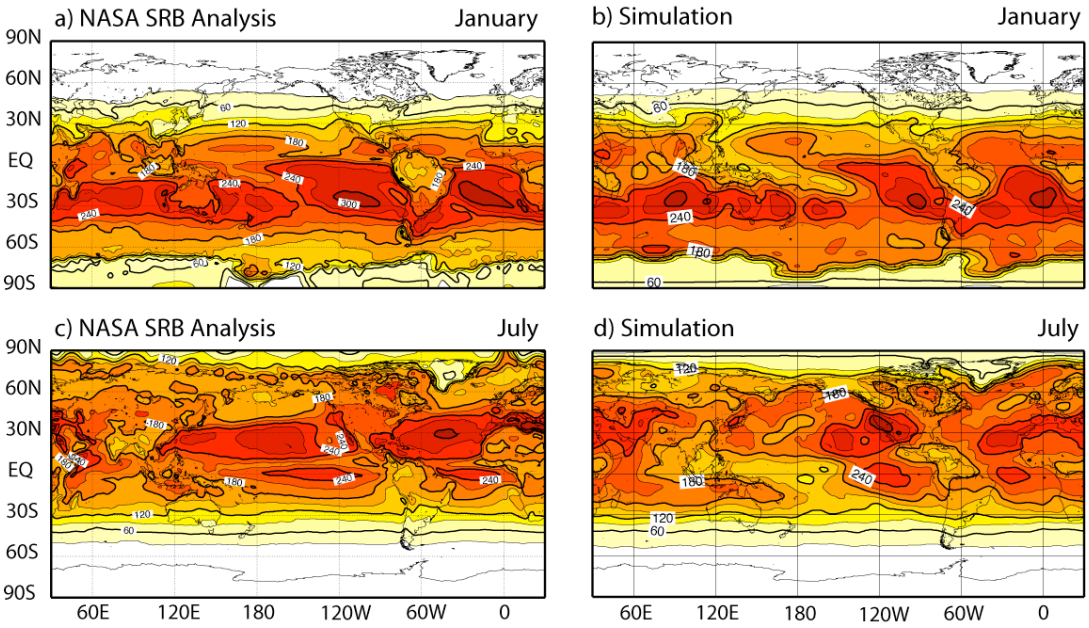

FIG. 6. Net short wave radiation flux (Wm^{-2}) at the surface from the NASA SRB analysis (left column) and simulations (right column) for January (upper row) and July (lower row). Downward flux is positive with 30 Wm^{-2} contour intervals.

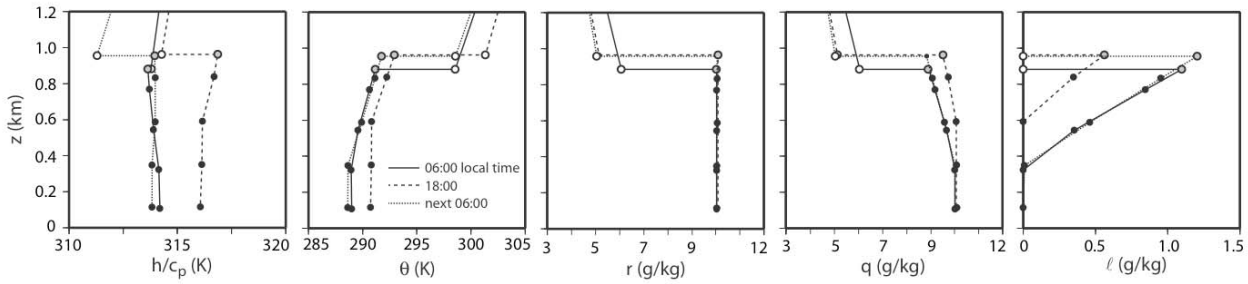

FIG. 7. Vertical profiles of moist static energy (left), potential temperature (second from left), total water mixing ratio (middle), water vapor mixing ratio (second from right) and liquid water mixing ratio (right).

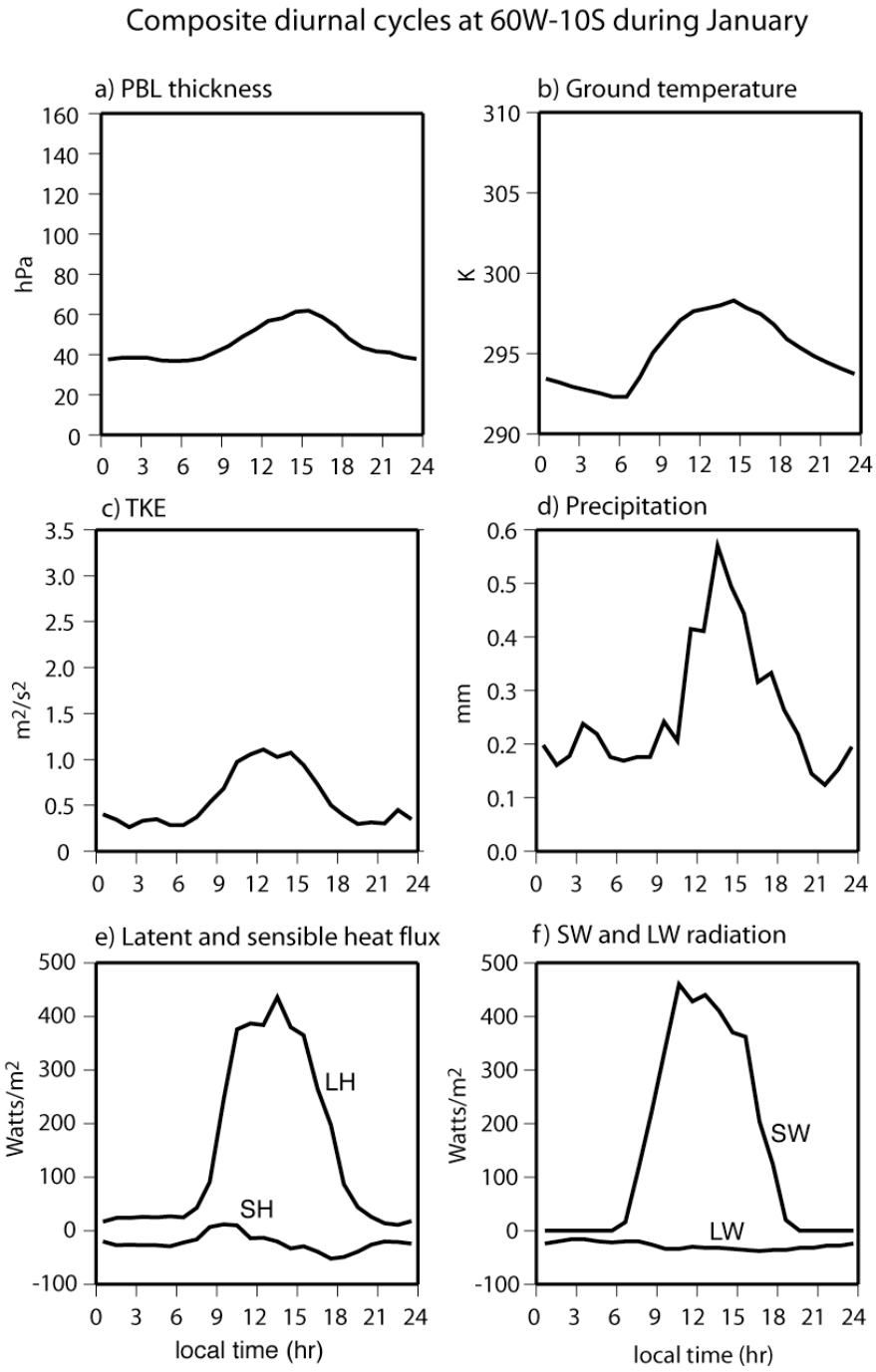

FIG. 8. Mean diurnal cycles at 60W-10S for January of (a) PBL thickness, (b) ground temperature, (c) TKE, (d) hourly precipitation rate, (e) upward latent and sensible heat flux at Earth's surface (curves indicated with "LH" and "SH", respectively) and (f) downward short and long wave radiation fluxes at Earth's surface (the curves indicated with "SW" and "LW", respectively). The diurnal cycles are given as function of local time.

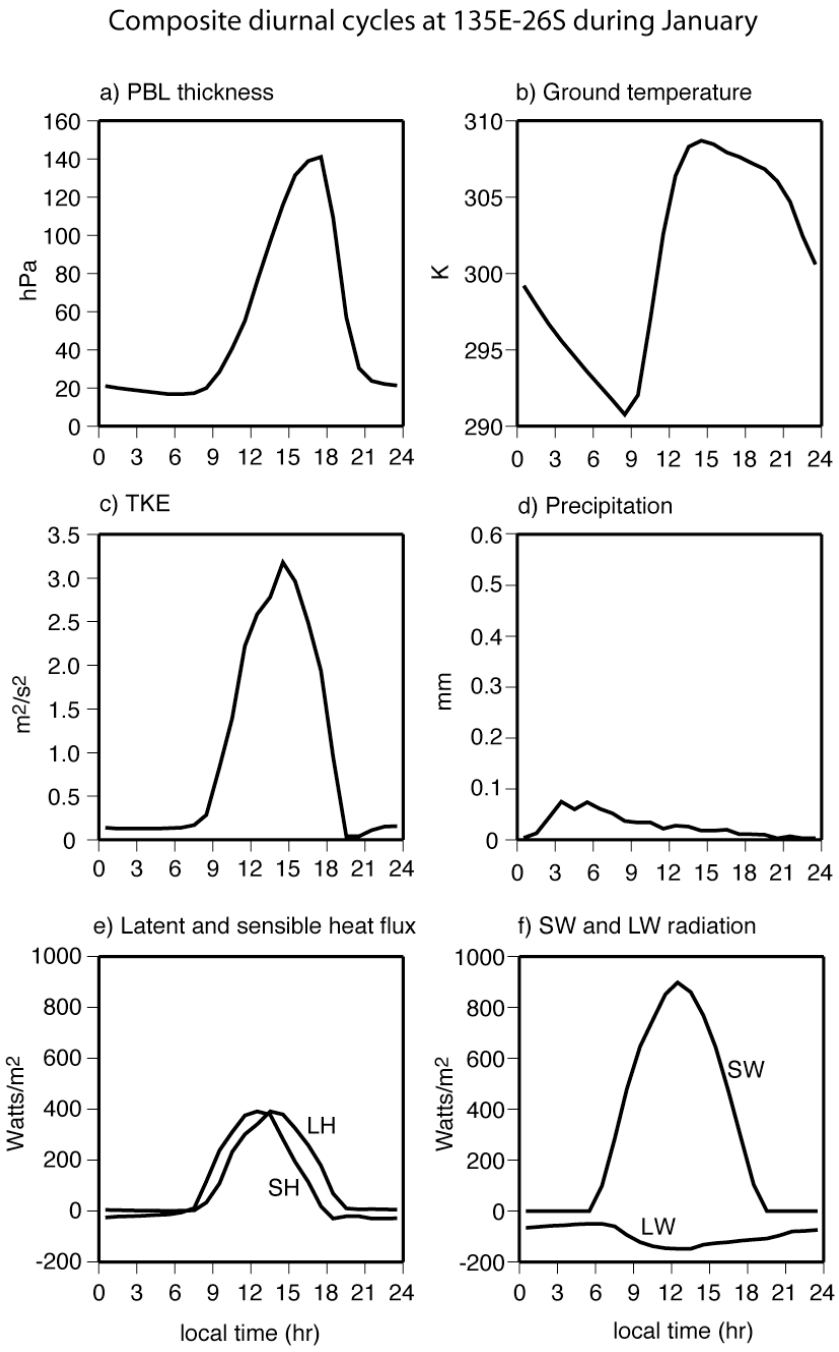

FIG. 9. Same as Fig. 8, except at 135W-26S.

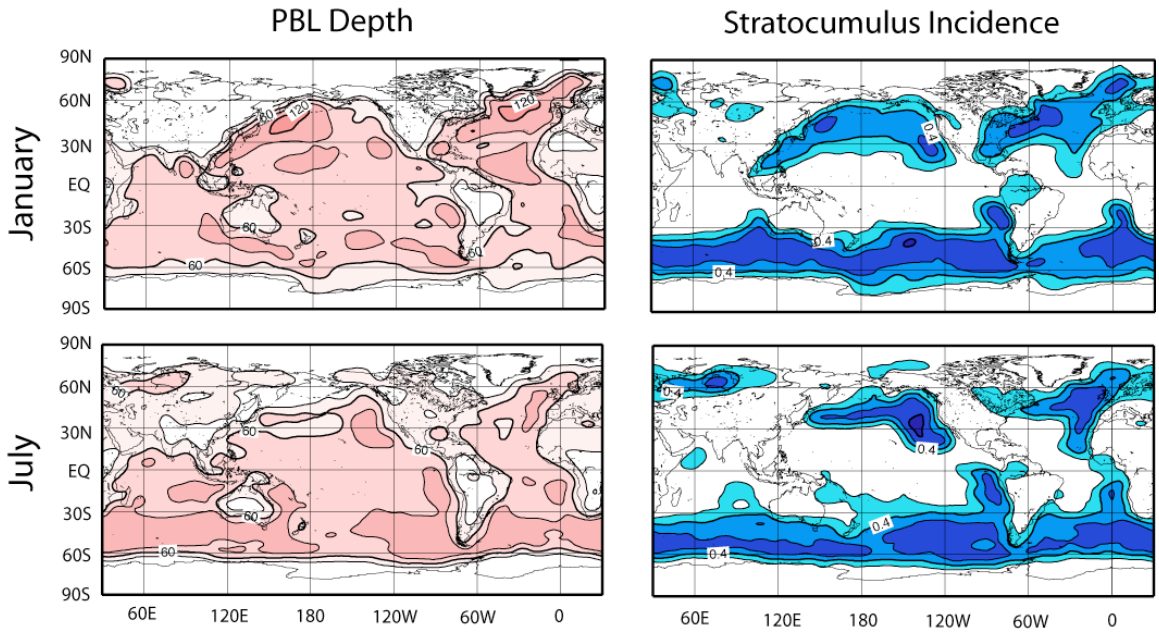

FIG. 10. Same as relevant panels of Fig.4, except for the SP simulation.

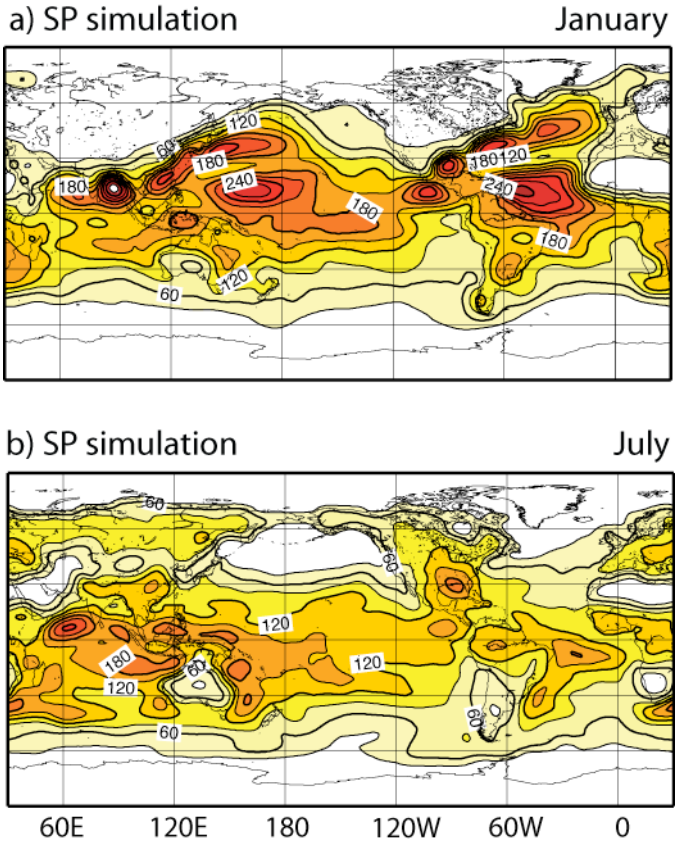

FIG. 11. Same as Fig.5, except for the SP simulation.

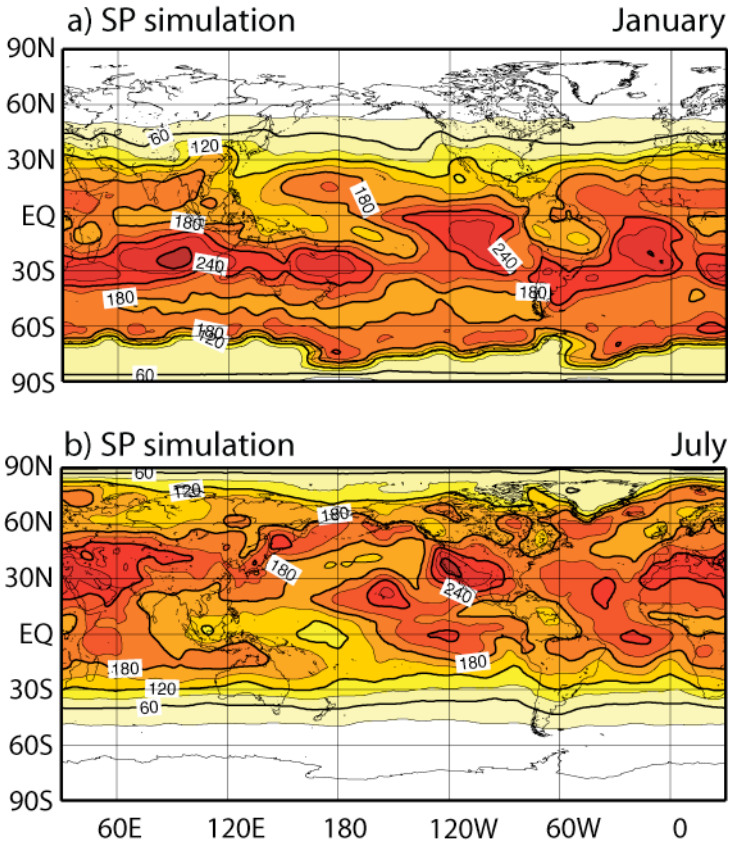

FIG. 12. Same as Fig.6, except for the SP simulation.

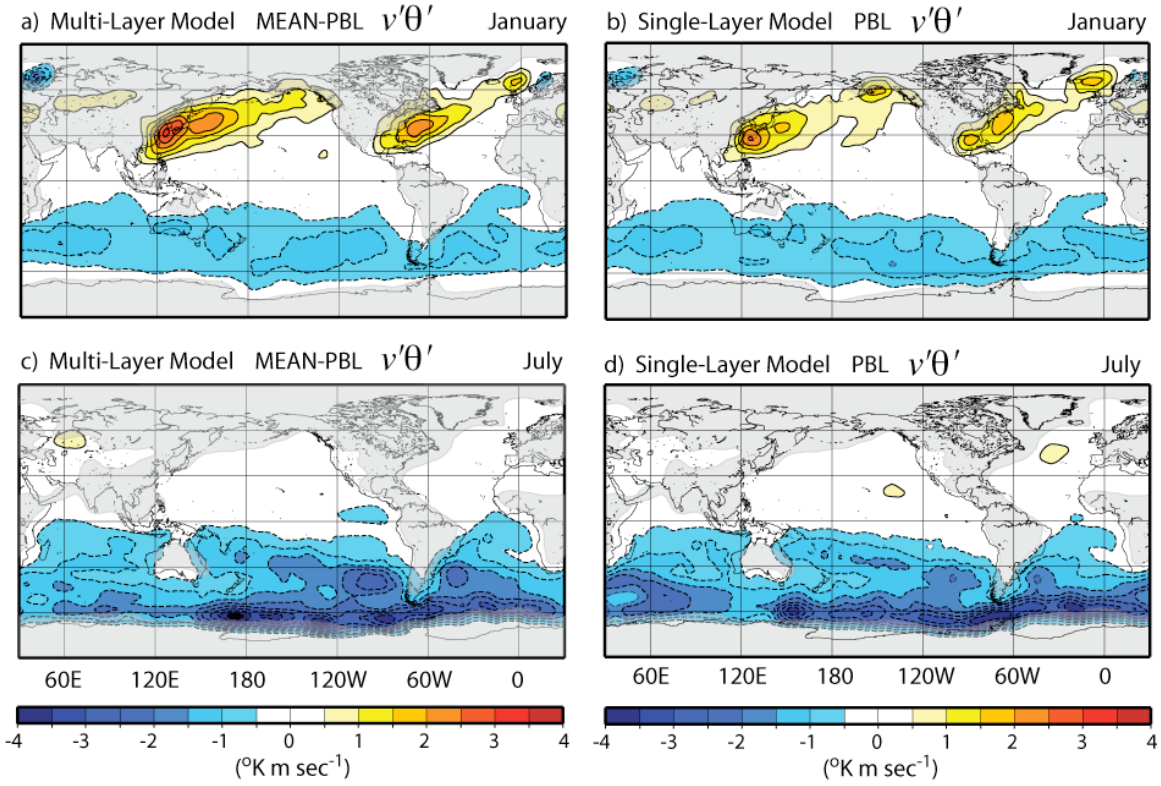

FIG. 13. Monthly-mean longitudinal potential temperature flux by eddies (^{o}Kmsec^{-1}). Upper and lower panels are for January and July, respectively. Left and right columns show results from the multi-layer CONTROL and single-layer simulation, respectively.

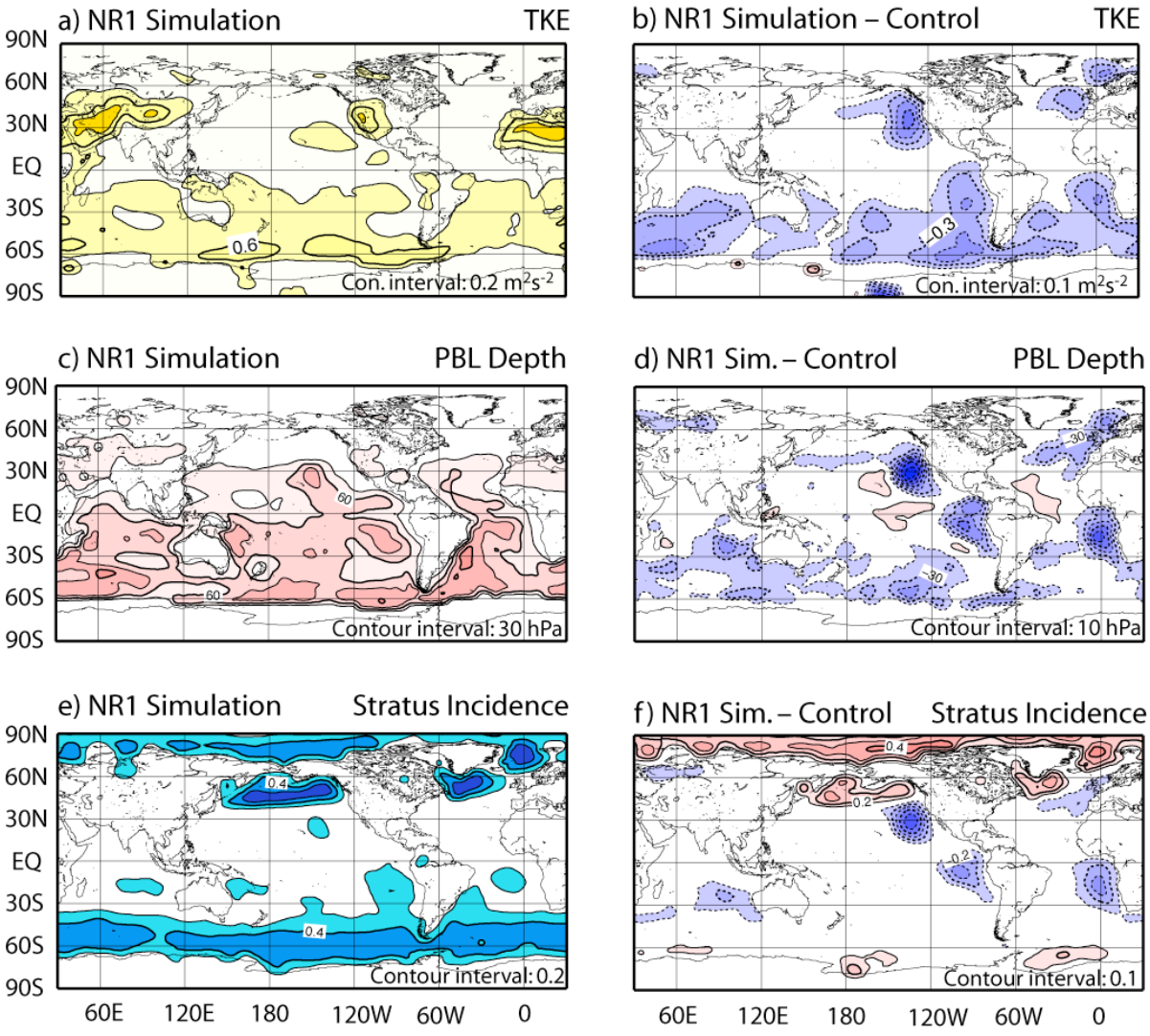

FIG. 14. Monthly-mean TKE (upper panel), PBL thickness (hPa, middle panel) and stratus incidence (lower panel) from the simulation with no radiative cooling effect in TKE and entrainment (NR1, left column) and difference between NR1 and Control (Fig. 4) simulations (right column).

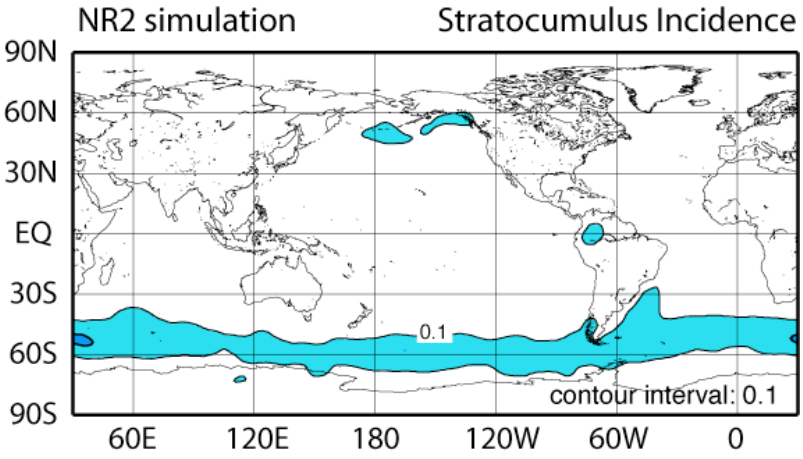

FIG. 15. Monthly-mean stratocumulus incidence from the simulation with no radiative cooling effect on TKE, entrainment and potential temperature for July (NR2 experiment).

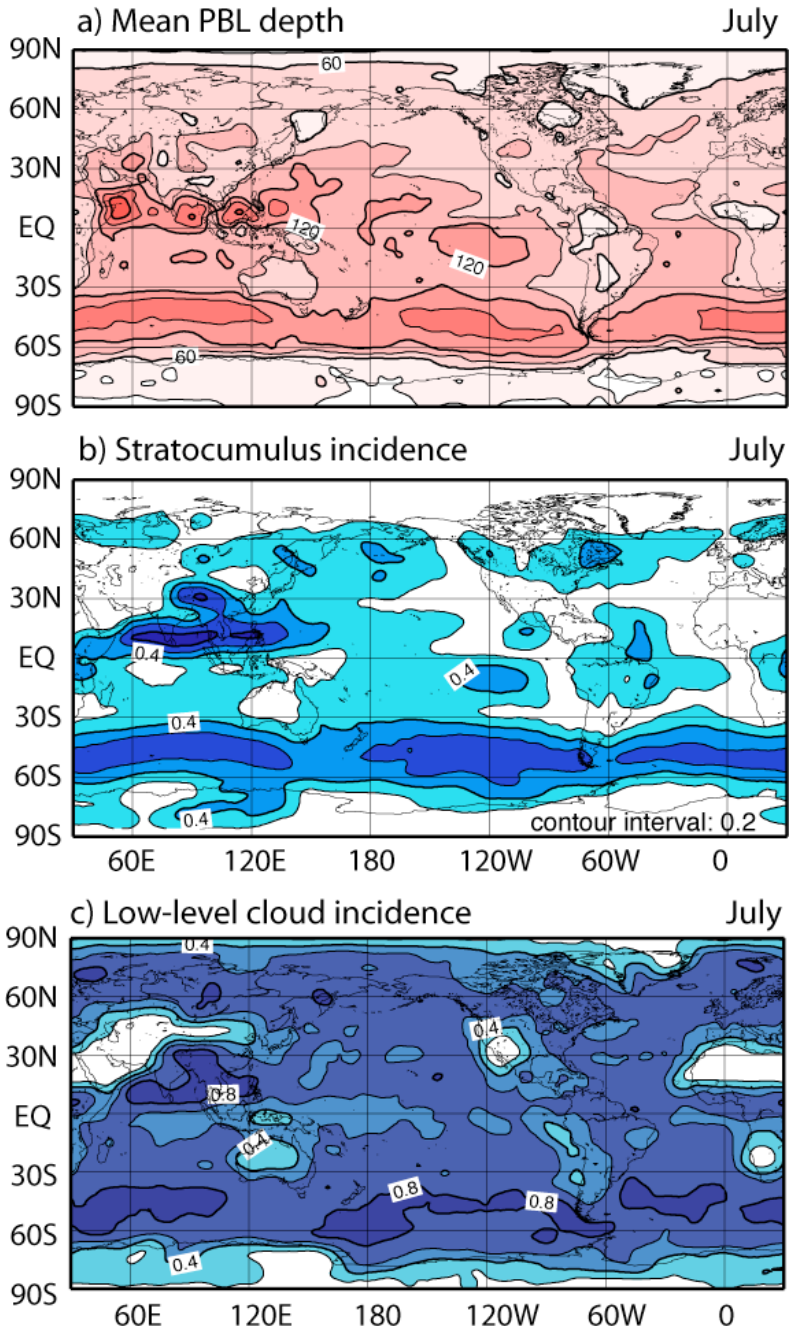

FIG. 16. (a) Monthly-mean PBL depth (hPa), (b) stratocumulus incidence (within the PBL) and (c) low-level cloud incidence (cloud incidence for the lowest 250 mb deep portion of the troposphere) for July from *fixed-sigma* simulation. See Fig. 4 for contour intervals.